JBC RESEARCH ARTICLE

The ubiquitin ligase Ariadne-1 regulates neurotransmitter release *via* ubiquitination of NSF

Received for publication, January 19, 2021, and in revised form, February 5, 2021 Published, Papers in Press, February 11, 2021,
https://doi.org/10.1016/j.jbc.2021.100408

Juanma Ramírez[1], Miguel Morales[2], Nerea Osinalde[3], Imanol Martínez-Padrón[2], Ugo Mayor[1,4,*], and Alberto Ferrús[2,*]

From the [1]Department of Biochemistry and Molecular Biology, Faculty of Science and Technology, UPV/EHU, Leioa, Bizkaia, Spain; [2]Cajal Institute, CSIC, Madrid, Spain; [3]Department of Biochemistry and Molecular Biology, Faculty of Pharmacy, UPV/EHU, Vitoria-Gasteiz, Araba, Spain; and [4]Ikerbasque, Basque Foundation for Science, Bilbao, Bizkaia, Spain

Edited by Phyllis Hanson

Ariadne-1 (Ari-1) is an E3 ubiquitin-ligase essential for neuronal development, but whose neuronal substrates are yet to be identified. To search for putative Ari-1 substrates, we used an *in vivo* ubiquitin biotinylation strategy coupled to quantitative proteomics of *Drosophila* heads. We identified 16 candidates that met the established criteria: a significant change of at least twofold increase on ubiquitination, with at least two unique peptides identified. Among those candidates, we identified Comatose (Comt), the homologue of the N-ethylmaleimide sensitive factor (NSF), which is involved in neurotransmitter release. Using a pull-down approach that relies on the overexpression and stringent isolation of a GFP-fused construct, we validate Comt/NSF to be an ubiquitination substrate of Ari-1 in fly neurons, resulting in the preferential monoubiquitination of Comt/NSF. We tested the possible functional relevance of this modification using Ari-1 loss-of-function mutants, which displayed a lower rate of spontaneous neurotransmitter release due to failures at the presynaptic side. By contrast, evoked release in Ari-1 mutants was enhanced compared with controls in a Ca^{2+}-dependent manner without modifications in the number of active zones, indicating that the probability of release per synapse is increased in these mutants. This phenotype distinction between spontaneous and evoked release suggests that NSF activity may discriminate between these two types of vesicle fusion. Our results thus provide a mechanism to regulate NSF activity in the synapse through Ari-1-dependent ubiquitination.

Neurotransmitter release is mediated by a set of protein–protein interactions that include the N-ethylmaleimide sensitive factor (NSF), soluble NSF attachment proteins (SNAPs), and SNAP receptors (SNAREs) (1). These proteins assemble into a tripartite complex in order to elicit synaptic vesicle fusion, which is formed by one synaptic vesicle membrane SNARE protein (v-SNARE), Synaptobrevin, and two plasma membrane SNARE proteins (t-SNAREs), Syntaxin and the 25-kDa synaptosome-associated protein (2). Following vesicle fusion, the tripartite SNARE complex disassembles by the activities of NSF and SNAPs (3). Free t-SNAREs from the plasma membrane can then participate in new priming reactions, while the v-SNAREs can be incorporated into recycled synaptic vesicles (4). These interactions, also routinely used for intracellular vesicle trafficking in all cell types, are conserved across species, including *Drosophila* (5).

Deviations on the rate of neurotransmitter release are at the origin of multiple neural diseases, including Parkinson's disease (6). Under physiological conditions, the Leucine-rich repeat Serine/Threonine-protein kinase 2 (LRRK2) phosphorylates NSF to enhance its ATPase activity, which facilitates the disassembly of the SNARE complex (7–9). However, the most common Parkinson's disease mutation in LRRK2 causes an excess of kinase activity (10) that interferes with the vesicle recycling (11). Similarly, α-Synuclein, another Parkinson's disease protein (12), alters neurotransmitter release by preventing the v-SNARE vesicle-associated membrane protein (VAMP)-2, also known as Synaptobrevin-2, from joining the SNARE complex cycle (13). Correct neural functioning, therefore, requires delicate regulation in vesicle trafficking. This regulation can be achieved by posttranslational modifications, such as ubiquitination. In fact, ubiquitination of certain proteins can affect their activity or life span (14, 15). At the presynaptic side, for example, increased neurotransmitter release correlates with decreased protein ubiquitination (16). Similarly, acute pharmacological proteasomal inhibition causes rapid strengthening of neurotransmission (17).

Ariadne 1 (Ari-1) is an E3 ubiquitin-ligase, first identified in *Drosophila* (18), from a conserved gene family defined by two C_3HC_4 *Ring* fingers separated by a C_6HC in-*Between-Rings* domain, the RBR motif (19). Ari-1 had been described to be essential for neuronal development, and its mutants reported to exhibit reduced eye rhabdomere surface and endoplasmic reticulum, as well as aberrant axonal pathfinding (18). However, despite its importance, no neuronal substrates have been reported so far. Only three Ari-1 substrates have been postulated, either in cultured cells or *in vitro* (20–22), while three Parkin substrates were reported to interact with Ari-1 in COS-1 cells (23). For this reason, with the aim to identify neuronal Ari-1 substrates, we took advantage of two methodologies

* For correspondence: Alberto Ferrús, aferrus@cajal.csic.es; Ugo Mayor, ugo.mayor@ehu.eus.
Present address for Miguel Morales: Orion Pharmaceutical, Turku, Finland.

developed by our lab (24). The first one, the ^{bio}Ub strategy, allows the identification of hundreds of ubiquitinated proteins from neuronal tissues (25, 26). The system relies on the overexpression of a tagged ubiquitin that bears a 16 amino acid long biotinylatable peptide (25, 27), which can be biotinylated by the *Escherichia coli* biotin holoenzyme synthetase enzyme (BirA) in neurons *in vivo* (25, 26). Remarkably, this approach can be efficiently applied to identify neuronal E3 ligase substrates (28, 29). The second methodology, in contrast, favors the isolation of GFP-tagged proteins under denaturing conditions to further characterize their ubiquitination pattern under the presence or absence of an E3 ligase (30, 31).

Here we have combined the ^{bio}Ub strategy with the overexpression of Ari-1 and identified 16 putative neuronal substrates of Ari-1. Among those, we focused on Comatose (Comt), the fly NSF orthologue (32), due to its relevance in normal and pathological function at the synapse. By the isolation of GFP-tagged Comt from *Drosophila* photoreceptor neurons overexpressing Ari-1, we confirmed Comt/NSF as an Ari-1 ubiquitin substrate and showed that it is mostly monoubiquitinated. Furthermore, we reported that Ari-1 loss-of-function mutants displayed lower rate of spontaneous neurotransmitter release, but enhanced evoked release, due to failures at the presynaptic side. These defects in the mutants are compatible with a deregulation of Com/NSF activity. Altogether, our data show that Ari-1 regulates neurotransmitter release by controlling Comt/NSF activity through ubiquitination.

Results

Generation of flies for the identification of neuronal Ari-1 substrates

We generated *GMR-Gal4, UAS-(^{bio}Ub)$_6$-BirA/CyO; UAS-ari-1/TM6* flies (hereinafter *ari-1^{OE}* flies, from Ari-1 overexpression) in order to screen, in an unbiased manner, for putative substrates of the E3 ligase Ari-1. These flies overexpress in photoreceptor neurons (using the *GMR-Gal4* driver) both an untagged version of Ari-1 protein (Fig. 1*A*) and the (^{bio}Ub)$_6$-BirA construct (Fig. 1*B*), which is the one that provides the biotinylatable ubiquitins and the BirA enzyme to the system. The rationale for using *GMR-Gal4* is that it has been shown to be a suitable driver for ubiquitin proteomics experiments from mature neurons, in comparison with other neuronal drivers tested (26). Flies only overexpressing the (^{bio}Ub)$_6$-BirA construct in photoreceptor neurons were used as control. Overall, expression levels of biotinylated ubiquitin were similar in both genotypes, as indicated by a western blot performed with biotin antibody using whole head extracts (see *input* fraction of Fig. 1*C*). Similarly, the amount of ubiquitinated material eluted from biotin pull-downs on both fly lines was also similar (see *elution* fraction of Fig. 1*C*).

Higher levels of Ari-1 enzyme in *ari-1^{OE}* flies should result in an enhanced ubiquitination of Ari-1 substrates relative to control flies. Therefore, quantitative proteomic experiments were carried out, following a previously described workflow (28, 29), to decipher the ubiquitinated proteome from both *ari-1^{OE}* and control flies and, hence, detect those proteins whose ubiquitination is regulated by Ari-1. In brief, we collected 500 mg of heads of each fly genotype and subjected triplicate samples to biotin pulldown and liquid chromatography with tandem mass spectrometry (LC-MS/MS) analysis. This allowed us to isolate, detect, and quantify ubiquitinated proteins present in fly photoreceptor neurons expressing physiological (control samples) and high (*ari-1^{OE}* samples) levels of Ari-1 (Fig. 1*D*). Only those proteins with at least a twofold enrichment, determined with a p-value < 0.05, in *ari-1^{OE}* samples were considered as putative Ari-1 substrates (Fig. 2*A*).

Identification of Ari-1 putative substrates by mass spectrometry

Biotin pull-downs were performed on three biological replicates for each condition. Identified ubiquitinated proteins were highly reproducible across the three replicate samples of each condition and also between both conditions (Fig. 2*B*). Protein abundance was determined using label-free quantification (LFQ) intensities (33), which also displayed a high correlation across samples (Pearson correlation ≥ 0.96). For statistical analysis, missing LFQ values were imputed with low random values from a normal distribution, meant to simulate expression levels below the detection limit. It should be noted that proteins with too many imputed LFQ values were discarded from the Ari-1 putative substrate list. Only proteins with LFQ values in at least the three replicas of one of the conditions, either *ari-1^{OE}* or control, or in at least two replicas of both conditions, are labeled in Figure 3.

Ari-1 protein was found significantly enriched (p = 0.0000176) in *ari-1^{OE}* samples relative to control flies (Ari-1, *ari-1^{OE}*/control LFQ ratio of 26.1) (Fig. 3). By contrast, and in agreement with western blotting results (Fig. 1*C*), ubiquitin levels were similar in both conditions (Ub, *ari-1^{OE}*/control LFQ ratio of 0.73) (Fig. 3). The relative abundance of the majority of proteins quantified did not change significantly either; this included Avidin (AVD) and proteins known to be endogenously conjugated with biotin (ACC: acetyl-CoA carboxylase, PCB: pyruvate carboxylase) (25, 34), which serve as internal controls to determine the correct processing of the biotin pull-downs (Fig. 3, marked in blue).

Out of the 1452 proteins quantified (see control *versus ari-1^{OE}* Venn diagram in Fig. 2*B*, and Table S1), 22 proteins were found significantly enriched (p-value < 0.05) by at least twofold ($\log_2$ fold change >1) in *ari-1^{OE}* flies relative to control flies (Fig. 3, marked in green), including the Ari-1 E3 ligase itself. Two proteins, Mdg3/ORF and Gag, correspond to products encoded by genes within a transposable element, whereas another two, Calx and MoxGM95, were only identified with one unique peptide. Additionally, Mccc1 had been classified as background in previous biotin pull-down experiments (26), as it uses biotin as cofactor. After excluding these proteins, the final list of putative Ari-1 substrates contained 16 proteins (Table 1). Four of these putative Ari-1 substrates are still uncharacterized *Drosophila* proteins (CG32486, CG32687, CG4629, and CG6424), but the remaining ones are involved in different metabolic processes (CG15117, GstO3, Lsp1β,

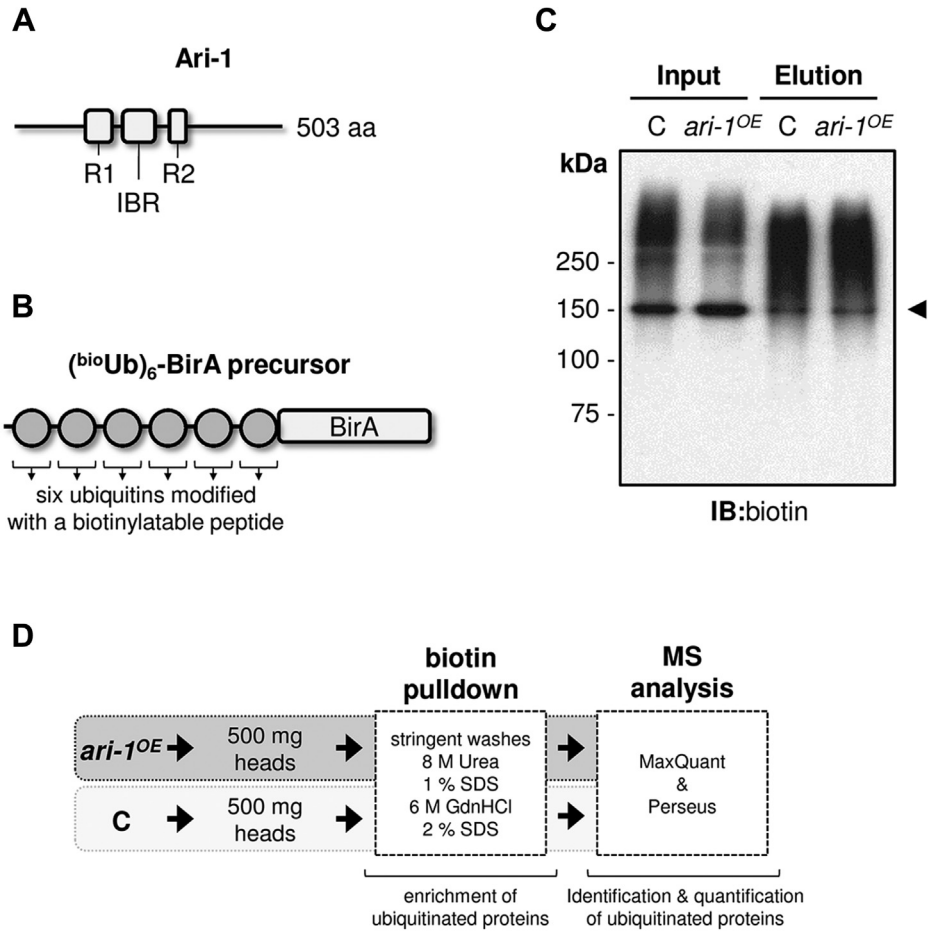

Figure 1. Generation of ^{bio}*ari* flies. *A*, schematic representation of the domain structure of *Drosophila* Ari-1 E3 ligase according to Uniprot (ID: Q94981). Ari-1 belongs to the RING between RING E3 ligase family, and as such, it is characterized by the presence of two RING domains (RING1 or R1 from residue 133–183 and RING2 or R2 from residue 291–322), which are separated by a conserved sequence called the in-between RING domain (IBR, from residue 203–264). *ari-1*^{OE} flies overexpress an untagged version of Ari-1 in the photoreceptor cells under the control of the *GMR-Gal4* driver. *B*, schematic representation of the (^{bio}Ub)$_6$-BirA precursor (25). It is composed of six copies of ubiquitin, which had been N terminus modified with a short biotinylatable peptide (MGLNDIFEAQKIEWHEGSGSG). The biotin holoenzyme synthetase (BirA) is found at the C terminus. This construct is digested by endogenous deubiquitinating enzymes, allowing the biotinylation of each ubiquitin molecule by BirA *in vivo*. Control and *ari-1*^{OE} flies overexpress this precursor in the photoreceptor cells under the control of the *GMR-Gal4* driver. *C*, expression of the biotinylated ubiquitin is similar between *ari-1*^{OE} and control (C) flies. Anti-biotin western blot performed on whole lysates (inputs), as well as on the fractions coming from biotin pulldowns, where the ubiquitinated material is enriched (elutions), is shown. The abundant pyruvate carboxylase (~130 kDa), which is biotinylated endogenously, is highlighted with an *arrowhead*. *D*, workflow for the identification of *Drosophila* Ari-1 substrates. In total, 500 mg of heads from *ari-1*^{OE} and control flies was subjected to biotin pull-downs and mass spectrometry analysis. MS data were analyzed by MaxQuant and Perseus softwares.

Oscillin, and PPO1), translation (EIFA), phototransduction (Rh4 and Rh6), ATP-hydrolysis coupled transmembrane transport (Vha 44 and Vha 68-1), and protein degradation (Prosα7). The putative Ari-1 substrate identified with the highest significance (p = 0.0000168) was Comt, a protein known to be involved in neurotransmitter release. The human orthologue of Comt, termed NSF (32), is known to regulate the disassembly of the SNARE complexes once neurotransmitter has been released (4).

The proteomics approach we applied does not particularly enrich for ubiquitination sites, nevertheless we did also identify 150 peptides containing the characteristic GlyGly remnant of ubiquitin. That is, the last two Glycines of ubiquitins that are left covalently attached to the substrates after trypsin digestion of the proteins (35). Of those, 64 GlyGly sites had been previously reported (26, 28, 29), but to our knowledge, 86 are novel ubiquitination sites not described until now in *Drosophila* (Table S1). Among the sites identified, we did also detect GlyGly remnants on the seven internal lysines of ubiquitin, which indicates that all ubiquitin type chains are present in fly neurons. The abundance of all ubiquitin chain types was comparable in control and Ari-1 overexpressing flies (Table S1), suggesting that high levels of Ari-1 do not alter the overall landscape of the ubiquitin linkages in flies, neither directly nor indirectly by affecting other ligases.

Comt is ubiquitinated by Ari-1 in Drosophila *neurons* in vivo

Having identified Comt as a putative substrate of Ari-1 by mass spectrometry analysis, we decided to validate this result biochemically. To that end, we combined flies that overexpressed a GFP-tagged version of Comt with the control and *ari-1*^{OE} fly lines previously used for the identification of putative Ari-1 substrates. The first combination gave rise to flies that overexpress the (^{bio}Ub)$_6$-BirA construct (Fig. 1*B*) together

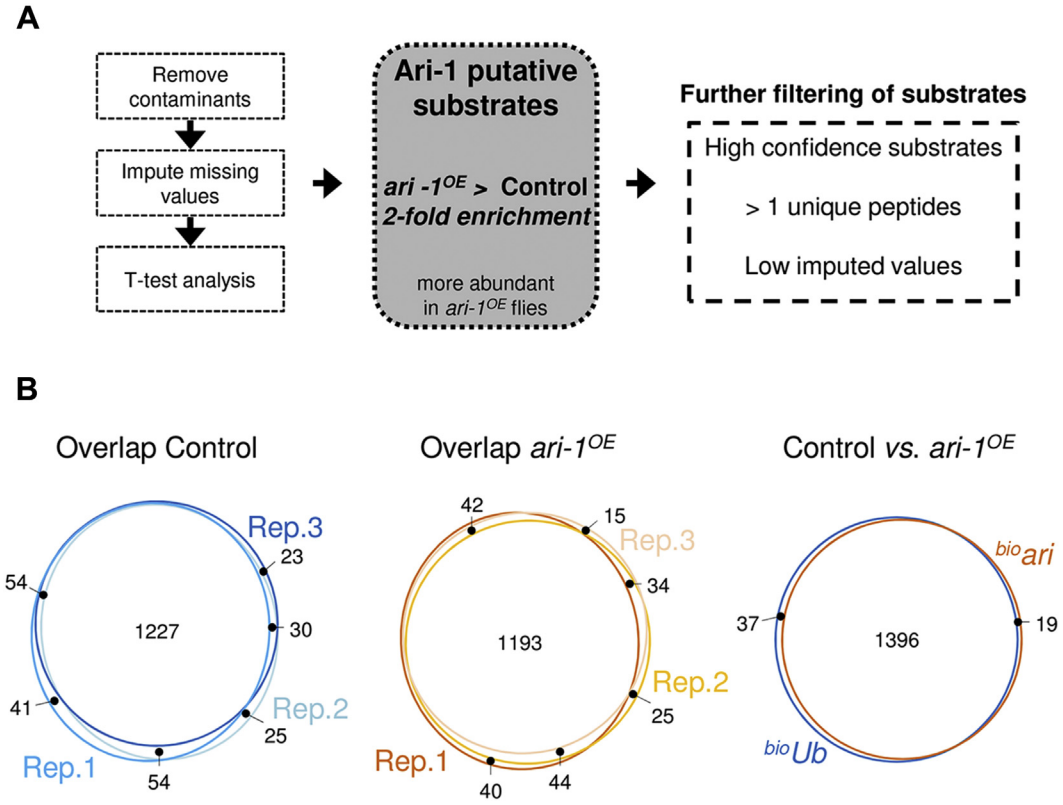

Figure 2. Mass spectrometry data analysis. *A*, workflow for selection of Ari-1 putative substrates. After removing contaminants, missing LFQ values were imputed and statistical significance determined by two-tailed Student's *t* test. Proteins with twofold enrichment in *ari-1*^{OE} samples relative to control were considered as putative Ari-1 substrates. These proteins were further filtered according to the number of peptides and the imputed values in order to obtain a list of high-confidence putative substrates. *B*, overlap between the MS-identified proteins from *ari-1*^{OE} and control samples. Venn diagrams displaying the overlap between the three *ari-1*^{OE} and control replicas, as well as between the two conditions are shown.

with GFP-tagged Comt, termed *comt* flies (Fig. 4*A*). The offspring of the second cross (the *ari-1*^{OE}*/comt* flies) express the Ari-1 E3 ligase (Fig. 1*A*), in addition to GFP-tagged Comt and the (^{bio}Ub)$_6$-BirA construct (Fig. 4*A*). We then performed GFP-pull-down assays (30) using protein extracts from *comt* and *ari-1*^{OE}*/comt* flies, in order to isolate GFP-tagged Comt and compare its ubiquitination levels in the presence of physiological (*comt*) or high levels of Ari-1 (*ari-1*^{OE}*/comt*) *in vivo*. After pull-downs, which were performed in triplicate, ubiquitinated and nonmodified fractions of Comt were monitored using anti-biotin and anti-GFP antibodies, respectively. We found a reduction of biotin and GFP signal in whole extracts of *ari-1*^{OE}*/comt* flies (Fig. S1*A*, input and Fig. S1*B*), which led to a reduction in the amount of eluted GFP-Comt protein from Ari-1 overexpressing flies compared with *comt* flies (Fig. S1*A*, elution original WB). This can be explained by a Gal4 dose effect, as the same dose of Gal4 protein is driving the expression of two and three UAS constructs in *comt* and *ari-1*^{OE}*/comt* flies, respectively (Fig. 4*A*). In fact, a reduced expression of the (^{bio}Ub)$_6$-BirA construct, measured with anti-BirA antibody, was also observed in *ari-1*^{OE}*/comt* flies compared with *comt* flies (Figs. S1 *A* and *B*). However, when comparable levels of eluted GFP-tagged Comt from each genotype were run on a gel, Comt was found highly ubiquitinated in the presence of Ari-1 (Figs. 4*B* and S1*A*, normalized WB). Interestingly, Ari-1 was found to preferentially enhance the monoubiquitination of Comt. It should be noted that monoubiquitination is a type of modification classically linked to the endocytosis of cell surface receptors (36, 37).

NSF is ubiquitinated by ARIH1 in HEK293 cells

Once confirmed that Comt is an Ari-1 substrates in flies, we aimed to test whether its human orthologue, NSF, is also ubiquitinated by the human Ari-1 E3 ligase orthologue, ARIH1. For that purpose, we generated a GFP-tagged version of NSF that was transfected in HEK293 cells, together with FLAG-tagged versions of either wild-type ARIH1 or catalytically inactive ARIH1 (Fig. 5*A*). The latter was generated by mutating its active site Cysteine at position 357 to a Serine (C357S), an amino acid that is able to bind ubiquitin but unable to transfer it to the substrates, as ubiquitin remains attached to the Serine through an oxyester bond (30, 38). In order to improve the detection of ubiquitin signal, cells were further transfected with FLAG-tagged ubiquitin (Fig. 5*A*). Cell extracts were subjected to GFP pulldown assay (30) and the ubiquitinated fraction of GFP-NSF analyzed by western blot. As expected, a significant reduction of the ubiquitinated levels of NSF was observed in the presence of the catalytically inactive ARIH1, confirming that NSF is also a substrate of human ARIH1 (Fig. 5*B*). Interestingly, like its fly counterpart,

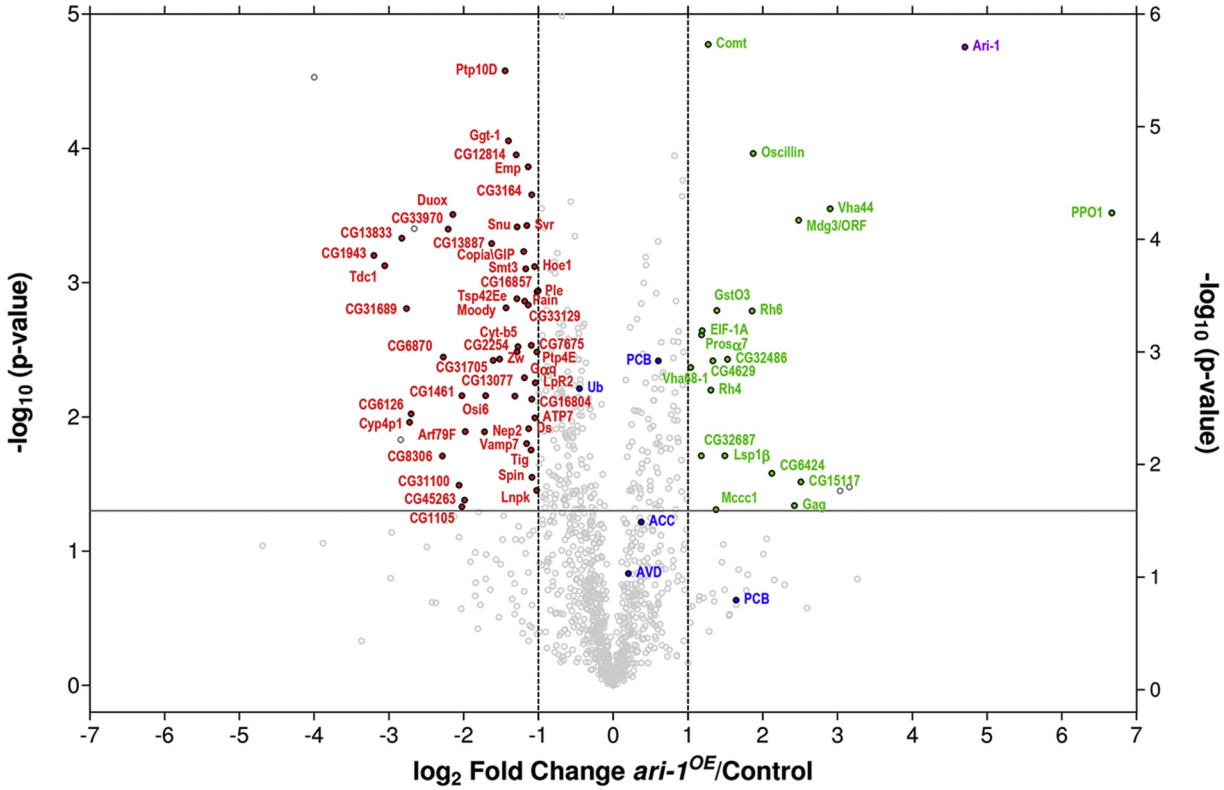

Figure 3. Putative Ari-1 substrates. Volcano plot showing differentially ubiquitinated proteins between *ari-1*^{OE} and control flies. Abundance of each individual protein was determined by the sum of LFQ intensities of the three replicas performed. LFQ *ari-1*^{OE}/Control ratios in the *x*-axis (in $\log_2$ scale) and the *t* test *p*-values in the *y*-axis (in $-\log_{10}$ scale) are displayed. The *horizontal gray lane* indicates the statistical significance (*p*-value < 0.05), while *vertical gray lanes* represent a twofold increase ($\log_2$ LFQ *ari-1*^{OE}/Control = 1) or a twofold decrease ($\log_2$ LFQ *ari-1*^{OE}/Control = −1), of the ubiquitination levels. Endogenously ubiquitinated proteins (ACC and PCB), Avidin (AVD), as well as ubiquitin (Ub) are shown in *blue*. Proteins whose ubiquitination increases or reduces at least twofold upon Ari-1 overexpression are shown in *green* and *red*, respectively. Ari-1 is shown in *purple*.

human NSF was also found to be preferentially mono-ubiquitinated in HEK293 cells. Altogether, these results confirmed that Comt/NSF is an *in vivo* target of Ari-1/ARIH1 E3 ubiquitin ligase, in both *Drosophila* and humans.

Ari-1 mutations alter spontaneous and evoked neurotransmitter release

Comt/NSF is a well-known component of the SNARE complex (3). SNARE complex formation bridges the vesicles and plasma membranes, mediating neurotransmitter release at synapses. As currently thought, NSF-SNAPs disassemble the SNARE complex by an ATP hydrolysis dependent process, allowing to recycle and to reuse SNARE components for a following round of vesicle fusion (5, 39). Consequently, we reasoned that Ari-1 might play a role in neurotransmission also. In order to test this hypothesis, we first analyzed spontaneous neurotransmitter release under two electrode voltage clamp conditions (TEVC). The frequency of spontaneous miniature events in neuromuscular junctions (NMJs) of *ari* mutant larvae was reduced over 50% relative to controls (Fig. 6, *A* and *B*) suggesting a presynaptic modification in mutant terminals. The mean of miniature excitatory junctional current (mEJC) frequencies in controls were 2.19 ± 0.26 Hz in normal larvae, 2.46 ± 0.29 Hz in the male *ari*^{2} mutant covered by the duplication *Dp(1;3)JC153 (ari*^{2}*; Dp)*, and 2.78 ± 0.26 Hz for the female siblings (*ari*^{2}/+ ♀). These genotypes constitute different forms of controls. By contrast, mEJCs in male mutant larvae were 1.02 ± 0.12 Hz for *ari*^{2}, 1.20 ± 0.38 Hz for *ari*^{3}, and 0.92 ± 0.12 Hz for *ari*^{4}. The reduced mEJC frequency of all *ari* mutant alleles indicates a relatively low rate of spontaneous synaptic vesicle fusion, which could arise from either a decreased number of release sites or a reduced probability of spontaneous vesicle fusion.

To further analyze spontaneous release, we compared the amplitude and time course of spontaneous mEJCs in *ari*^{2} ♂ *versus ari*^{2}/+ ♀ larvae (Fig. 6*C*). The mean *ari*^{2} mEJC peak amplitude (0.73 ± 0.007 nA, n = 7 cells) was not significantly different from that of *ari*^{2}/+ controls (0.75 ± 0.02 nA, n = 7). Cumulative frequency distribution of mEJC amplitudes (Fig. 6*C*) also revealed not significant differences between *ari*^{2} ♂ and *ari*^{2}/+ ♀ larvae. Further, both genotypes showed a very similar mEJC time course (Fig. 6*C*, inset). The fact that mEJC amplitude and time course remain the same in *ari*^{2} indicates that postsynaptic glutamate receptor properties and receptor density per active site are not altered and further reinforce the hypothesis that the primary mutant defect is at the presynaptic site.

We also noticed a conspicuous enlargement of evoked release in *ari*^{2} mutants. Postsynaptic evoked synaptic currents (EJC) in *ari*^{2} males were larger than those of the heterozygous female controls (Fig. 6*D*). To characterize in detail these effects, EJCs

Table 1
High confidence putative Ari-1 substrates

Name[a]	MW (kDa)	FC	*p*-value	Unique peptides	Biological process	Orthologue[b]
PPO1	79	101.70	3.03E-04	7	Dopamine metabolic process	-
Vha44	92	7.46	2.81E-04	3	Proton transmembrane transport	ATP6V1C1
CG15117	71	5.69	3.05E-02	2	Carbohydrate metabolic process	GUSB
CG6424	88	4.35	2.63E-02	6	-	FAM13A
Oscillin	29	3.66	1.09E-04	3	Glucosamine catabolic process	GNPDA2
Rh6	41	3.62	1.63E-03	2	Phototransduction	OPN4
CG32486	45	2.88	3.72E-03	6	-	CYHR1
Lsp1β	95	2.82	1.95E-02	2	-	-
GstO3	27	2.61	1.62E-03	2	Glutathione metabolic process	GSTO1
CG4629	63	2.52	3.82E-03	11	Protein phosphorylation	NIM1K
Rh4	42	2.47	6.32E-03	6	Phototransduction	OPN4
Comt	82	2.41	1.68E-05	26	SNARE complex disassembly	NSF
EIF-1A	17	2.28	2.28E-03	4	Translation	EIF1AY
Prosα7	27	2.27	2.45E-03	8	Proteasomal catabolic process	PSMA3
CG32687	41	2.27	1.95E-02	3	-	LRRC58
Vha68-1	68	2.05	4.29E-03	16	Proton transmembrane transport	ATP6V1A

Fly protein names. sizes (MW), unique peptides, and the biological process they are involved in are reported. *ari-1*^{OE}/control fold changes (FC) and its statistical significance (*p*-value) are also given. The complete data set, as well as all GlyGly peptides, is available as Supporting information in Table S1.
[a] Given according to Flybase nomenclature (https://flybase.org/).
[b] Humna orthologues with the best Flybase score are provided.

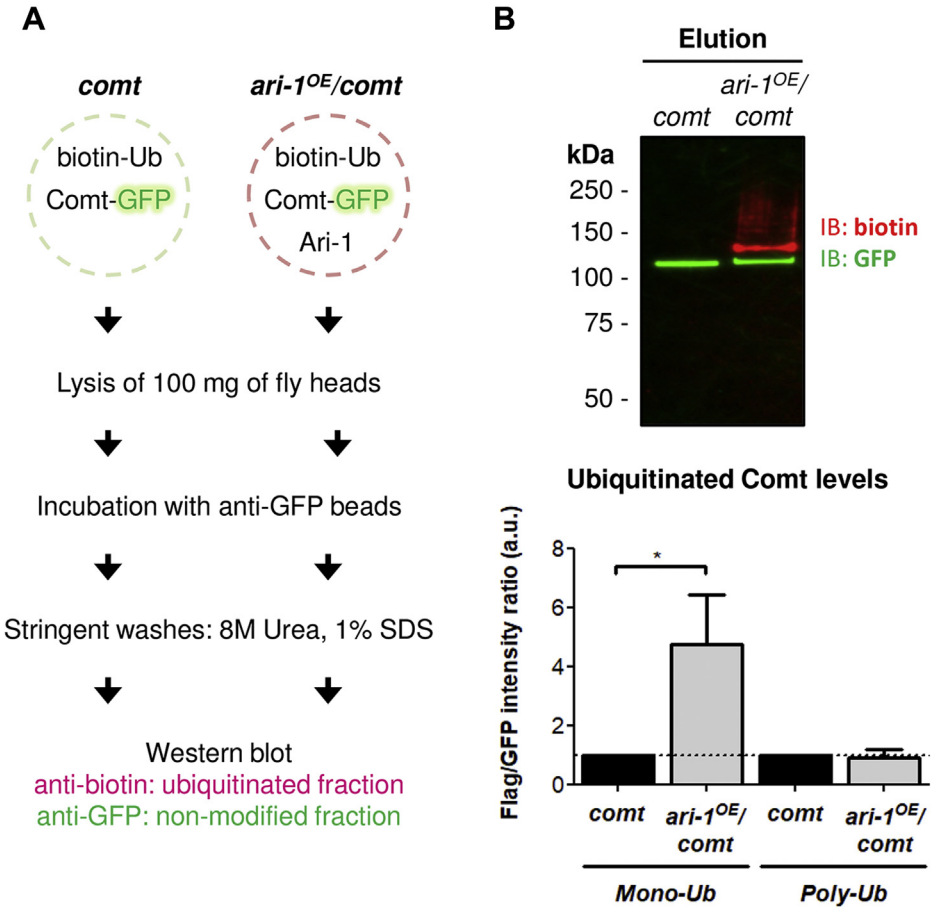

Figure 4. Validation of Comt as an Ari-1 substrate. *A*, workflow for the validation of Comt as Ari-1 substrate. *comt* flies express the (^{bio}Ub)$_6$-BirA construct (biotin-Ub; see Fig. 1*B*) and a GFP-tagged version of Comt (Comt-GFP) under the control of the neural photoreceptor expressed *GMR-Gal4* driver. *ari-1*^{OE}/*comt* are *comt* flies that express, in addition, the Ari-1 E3 ligase. In total, 100 mg of head of each genotype was lysed and incubated with anti-GFP beads in order to isolate GFP-tagged Comt. After stringent washes with 8 M Urea and 1% SDS, the ubiquitination levels of GFP-tagged Comt in both genotypes were determined by western blot with anti-biotin antibody. Nonmodified GFP-tagged Comt was monitored with anti-GFP antibody. *B*, Comt-GFP is ubiquitinated by Ari-1. Western blot performed on isolated GFP-tagged Comt in the presence of physiological (*comt*) or high levels of Ari-1 (*ari-1*^{OE}/*comt*). Equal levels of GFP-tagged Comt were loaded in order to have comparable ubiquitinated levels. Ubiquitinated fraction (*red*) was monitored with anti-biotin antibody, while anti-GFP was used to detect the nonmodified fraction (*green*). Below, a quantification of both mono and polyubiquitinated forms of GFP-tagged Comt from three independent pulldowns is shown. Semiquantification of dual-color western blots was performed with Image Lab software (Bio-Rad), ubiquitination levels of GFP-tagged Comt (*red*) were normalized to the nonmodified fractions (*green*) and statistical significance determined by two-tailed Student's *t* test. In this graph ubiquitinated Comt levels in *ari-1*^{OE}/*comt* flies were additionally normalized to the levels found in control flies (*comt*) for a clearer representation; in *comt* flies ubiquitinated levels are, therefore, shown as 1 (*dash horizontal line*). *p-value = 0.0146.

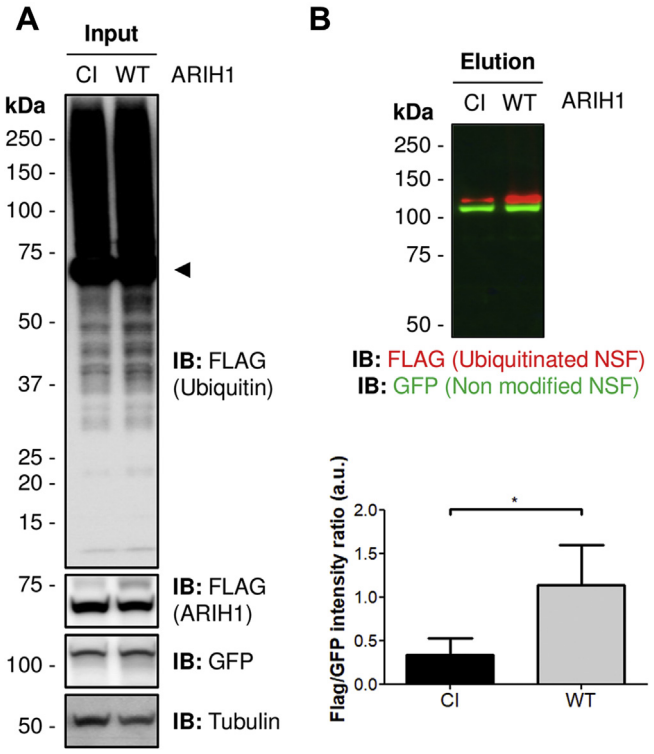

Figure 5. Validation of human NSF as an ARIH1 substrate. *A*, western blot on HEK293 whole cell extracts. HEK293 cells were cotransfected with FLAG-tagged ubiquitin, GFP-NSF, and either FLAG-tagged ARIH1^{WT} (WT) or the catalytically inactive ARIH1$^{C\ 357S}$ (CI) E3 ligase. GFP-NSF levels were detected with anti-GFP antibody. FLAG-ubiquitin and FLAG-ARIH1 levels (*arrowhead* in the *upper panel*) were detected with anti-FLAG antibody. Tubulin was used as loading control. *B*, GFP-NSF is ubiquitinated by ARIH1. Western blot performed on isolated GFP-tagged NSF in the presence of wild-type ARIH1 (WT) or a catalytically inactive ARIH1 (CI). Ubiquitinated fraction (*red*) was monitored with anti-FLAG antibody, while anti-GFP was used to detect the nonmodified fraction (*green*). Below, a quantification of GFP-tagged NSF from three independent pulldowns is shown. Semi-quantification of dual-color western blots was performed with Image Lab software (Bio-Rad) and statistical significance determined by two-tailed Student's *t* test. **p*-value = 0.0177.

amplitudes were analyzed at various extracellular Ca^{2+} concentrations (from 0.3 to 1.2 mM) by stimulating the fibers at 0.2 Hz. In all Ca^{2+} concentrations tested, *ari*^{2} ♂ EJC amplitudes were larger than those of the female controls, although differences reached statistical significance at 1.2 and 0.90 mM only (Fig. 6*E*). Thus, in the presence of 1.2 mM extracellular Ca^{2+}, the mean peak EJC amplitude for *ari*^{2} ♂ was 124.61 ± 9.72 nA (n = 6) compared with 77.20 ± 5.33 nA, (n = 6) for *ari*^{2}/+ females. Similar differences were found at an extracellular Ca^{2+} concentration of 0.90 mM (*ari*^{2} ♂: 73.3 ± 9.5 *versus* 43.2 ± 4.3 nA in *ari*^{2}/+ ♀) while at lower concentrations: 0.6 mM (*ari*^{2} ♂: 19.2 ± 6.8 *versus* 12.2 ± 1.6 nA in *ari*^{2}/+ ♀), 0.45 mM (*ari*^{2} ♂: 5.2 ± 1.7 *versus* 2.9 ± 0.5 nA in *ari*^{2}/+ ♀), and 0.3 mM (*ari*^{2} ♂: 1.0 ± 0.2 *versus* 0.5 ± 0.0 nA in *ari*^{2}/+ ♀) differences were not statically significant.

Short-term synaptic depression observed during long high-frequency stimulation is associated with the slower replenishment of the readily releasable pool (RRP) (40), reflecting the number of vesicles docked and ready to be released. Accordingly, rapid stimulation depletes the RRP and the subsequent responses rely on the replenishment of the RRP. In order to examine the possible effects of *ari* over the whole synaptic refilling process, we employed a 10 Hz stimulation protocol to monitor synaptic vesicle replenishment (Fig. 6*F*). The average results of six different experiments did not show any difference between *ari*^{2} ♂ and its sibling female controls.

A larger EJC can be explained by a relative large number of synaptic release sites. To discard this possibility, the number of synaptic contacts was analyzed and compared (Fig. 7, *A* and *B*). We found that the total number of synaptic contacts onto muscle fibers 6/7 (abdominal segment 3) in *ari*^{2} ♂ (82.55 ± 4.37, n = 20) was not significantly modified with respect to female controls *ari*^{2}/+ ♀ (79.72 ± 3.62, n = 22). Actually, no obvious morphological difference in NMJs between mutant and control larvae could be found.

The fact that evoked synaptic release is increased in *ari*^{2} ♂ while exhibiting a similar number of synaptic contacts would argue for an upregulation of quantal release per synapse. To explore this possibility, we performed a failure test analysis (41), by means of focal recordings of single boutons (type Is) (42) while simultaneously recording the muscular depolarization (EJP: Excitatory Junctional Potential) from the corresponding muscle fiber (Fig. 7, *C* and *D*). The Ca^{2+} concentration in the bath and inside the pipette was the same (0.6 mM nominal). The rate of synaptic failures was set to yield about a 50% failure rate in control animals by adjusting the stimulation potential. Under this condition 52.1 ± 4.2% (n = 8 recording sites from eight different animals) of stimuli failed to elicit neurotransmitter release in *ari*^{2}/+ ♀ animals, whereas in *ari*^{2} ♂ mutants, transmitter release failed only in 30.1 ± 4.9% (n = 8) of the cases (Fig. 7*D*). This difference is statistically significant (p = 0.0054) and indicates that mutant boutons release more neurotransmitter in response to nerve stimulation.

We considered two possible mechanisms to explain this enhancement: (1) mutant boutons contain larger amounts of transmitter release machinery and therefore more release sites, and (2) the probability of vesicle fusion in response to calcium at each release site is increased in the mutant. To distinguish between these two alternatives, we examined transmitter release from single varicosities at very high calcium concentrations. The rationale behind is that, at a calcium concentration that saturates the release machinery, most release sites would be recruited during nerve stimulation, and the amplitude of the synaptic response would mainly be governed by the number of release sites.

For these experiments, the bathing solution and the focal pipette contained 0 and 20 mM calcium, respectively (Fig. 7*E*). The calcium-containing pipette was placed over single type Is boutons, and the EJP was recorded with an intracellular electrode (Vm in the range of −35 mV to −40 mV, Fig. 7*E*). Each EJP amplitude data was the average of 20 consecutive responses from the same bouton, elicited at 0.1 Hz intervals, provided that no trend toward synaptic response decrement was observed. The amplitudes of the intracellular recorded EJPs were 4.1 ± 0.3 (n = 6 recording sites from six different animals) and 4.2 ± 0.5 (n = 5) in control and mutant animals, respectively (Fig. 7*F*); the difference not being statistically significant. These results indicate that, under conditions of elevated probabilities of release, mutant terminals do not

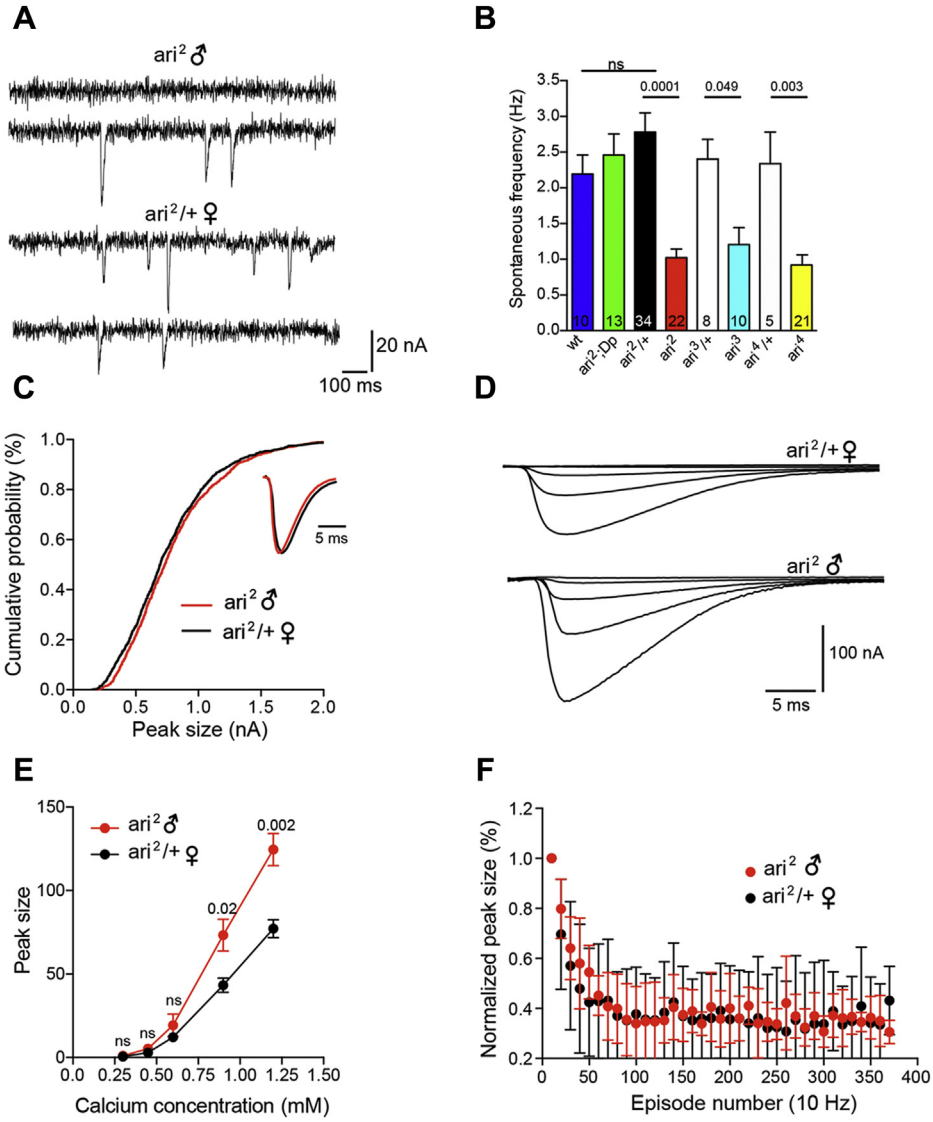

Figure 6. Synaptic release is affected in *ari-1* mutants. *A*, mEJC frequency in *ari-1* mutants is reduced. Representative traces from a spontaneous mEJCs recording. Events were captured under TEVC (Vh = −80 mV) from larval muscle 6 fibers in *ari*^{2} mutant male (*top*) and in heterozygous *ari*^{2}/+ female siblings (*bottom*). *B*, quantification of the effects over spontaneous release. mEJC frequency (mean ± SEM) was calculated from the following larvae strains; (wt), *ari*^{2}♂ covered by the duplication *Dp(1;3)JC153* (*ari*^{2}*;Dp*), heterozygous *ari*^{2} female siblings (*ari*^{2}/+ ♀), *ari*^{2} ♂ and two additional *ari* alleles (*ari*^{3} and *ari*^{4}), and their respective heterozygous females. Student's *t* test. Note the consistent reduction of mEJC frequency across all mutant genotypes with respect to the sibling female controls. *ari*^{2} is a C150Y mutation in the first R motif of the RBR domain; *ari*^{3} is a C309Y mutation in the second R motif; and *ari*^{4} is a point mutation that generates a STOP codon at amino acid 91. *C*, neither size nor mEJC time course is affected in *ari*^{2} animals. Cumulative probability curve of mEJC amplitudes for *ari*^{2}/+ ♀ (*black*) and *ari*^{2} ♂ (*red*) larvae (n = 7 larvae). Inset: average representative mEJC traces from *ari*^{2} ♂ mutant superimposed to that of *ari*^{2}/+ ♀. Traces were scaled up to the maximum peak value. *D*, representative traces of evoked transmitter release recorded under TEVC (Vh = −80 mV), at increasing extracellular Ca^{2+} concentrations (from 0.3 to 1.2 mM), recorded from sibling *ari*^{2}/+ ♀ and *ari*^{2} ♂ larvae. *E*, quantification of Ca^{2+} dependence of evoked release. Maximal EJC response was plotted *versus* the extracellular calcium concentration for *ari*^{2} ♂ compared with *ari*^{2}/+ ♀ (n = 6 for all genotypes; one-way ANOVA post hoc: Student's *t* test). *F*, quantification of EJC trains in response to a 10 Hz stimulation. Peak size was normalized to their initial response. Average of six different experiments from *ari*^{2} ♂ and *ari*^{2}/+ ♀ larvae.

release more transmitter than controls. We interpret this result in the sense that the number of release sites per bouton is not modified in the mutant and favor the hypothesis of a regulatory mechanism that increases transmitter release probability at physiological calcium concentration.

Ari-1 and comt mutants interact in vivo

In order to assay if the proposed interaction between Ari-1 and Comt would reflect in phenotypic changes at the whole organism level, we analyzed the thermo-sensitive paralysis and recovery of the *comt*^{6} allele, a single amino acid substitution, P398S, in Comt mutant background. To that end, we recombined *comt*^{6} with *ari*^{2} and monitored the paralysis at 37 °C and recovery times at room temperature of *comt*^{6}*/comt*^{6} *versus comt*^{6} *ari*^{2}*/comt*^{6} females (Fig. 8). The data show that, although paralysis time was not affected by the presence of *ari*^{2} in one dose, the recovery time was severely extended in comparison to *comt*^{6} alone. As control, the *comt*^{6} *ari*^{2}*/FM7* or *ari*^{2}*/FM7* females did not paralyze at all. Noticeably, the *comt*^{6} *ari*^{2}*/comt*^{6} females during the recovery time show uncoordinated movement of legs and some of them

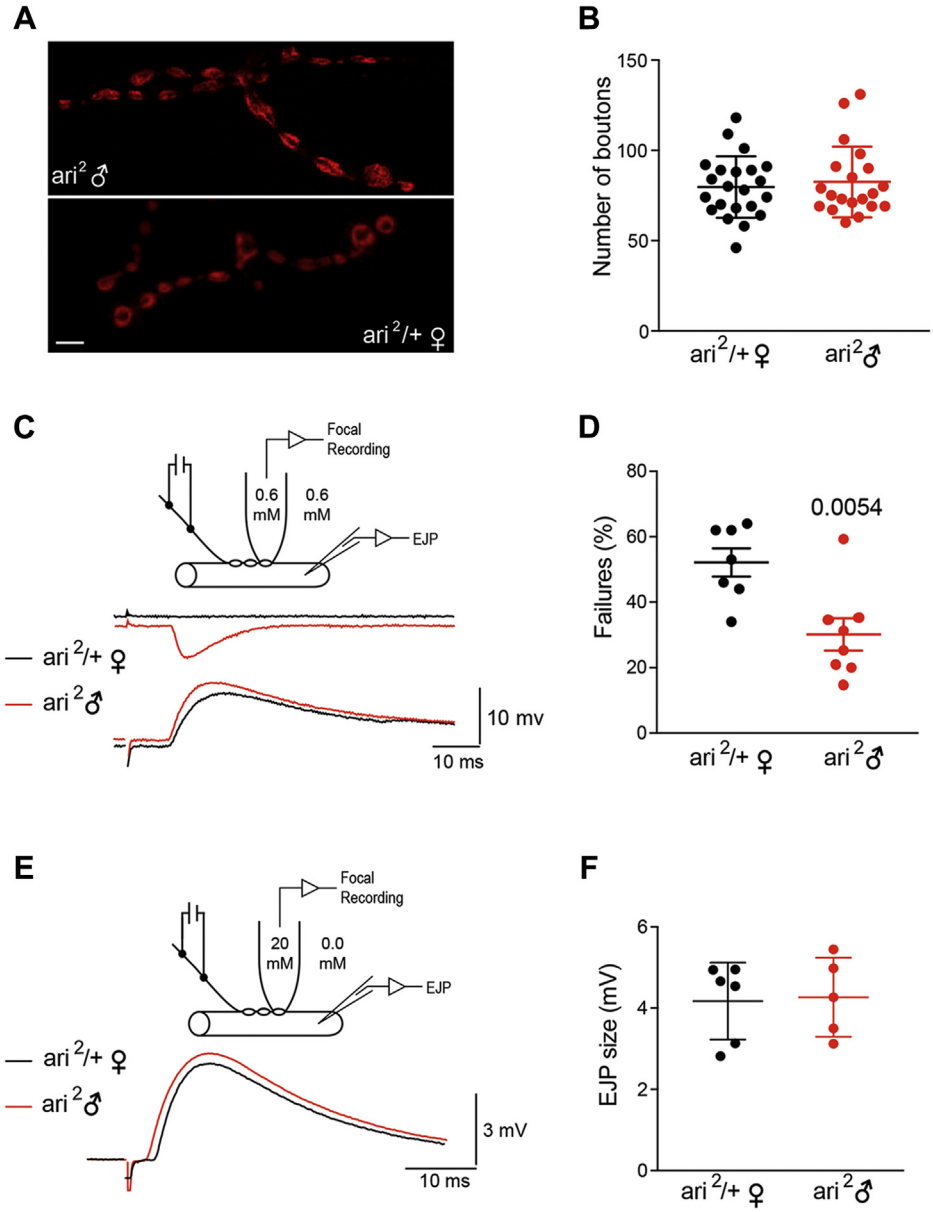

Figure 7. *Ari-1* mutants have low synaptic failure rate. *A*, synaptic density is not affected by *ari*^{2} mutation. Synaptic boutons were identified by inmunostaining against the presynaptic protein CSP. Representative confocal images from *ari*^{2} ♂ mutant (*top*) and control (*bottom*) neuromuscular junctions (muscle 6). Bar = 10 μm. *B*, the average number of synaptic boutons in larval motorneurons from *ari*^{2} ♂ compared with the sibling heterozygous *ari*^{2}/+ ♀ are not statistically different. *C*, *ari*^{2} ♂ mutants have fewer transmitter release failures. *Top drawing*: scheme of the recording. An extracellular focal recording of the synaptic current (type Is) is done by the help of a patch pipette placed over the presynaptic terminal. Calcium was kept at the same extracellular concentration (0.6 mm). The excitatory junction potential (EJP) was recorded from the muscle fiber. *Bottom*: representative traces of a simultaneous focal and EJP recording. In *red*, an *ari*^{2} ♂ recording, superimposed to a female *ari*^{2}/+ ♀ (*black traces*). Note how a single bouton failure correlates with a normal EJP at the muscle fiber level, indicating that it represents a true failure to recruit the release sites under the focal recording pipette. *D*, the mean average number of failures was smaller in the *ari*^{2} ♂ mutants (n = 8) when compared with the heterozygous *ari*^{2}/+ ♀ (n = 8). Student's *t* test. *E*, in *ari*^{2} mutants, the release probability is higher in physiological calcium concentrations. *Top drawing*: scheme of the recording. Extracellular calcium was kept at 0 mM nominal concentration to inhibit release, while the presynaptic bouton under the focal recording was kept at 20 mM to maximize release probability. *Bottom*: representative average evoked EJPs recorded in muscle fiber 6 from *ari*^{2} ♂ mutants (*red*) and control larvae *ari*^{2}/+ ♀ (*black*). Each trace is the average of 20 consecutive recordings at 0.1 Hz stimulation. To reduce calcium dilution inside the pipette, we employed a fresh pipette every time and proceeded with the experiment as quickly as possible. *F*, average EJP amplitudes corresponding to data collected from *ari*^{2} ♂ mutants (n = 5) and *ari*^{2}/+ ♀ controls (n = 6). The average size was not different when release probability was increased.

required more than 1 h to reach the standup criterion (see Experimental procedures). These flies, however, eventually recover and exhibit normal movements including jump and flight. This feature is compatible with the requirement of Ari-1 activity upon NSF in various aspects of the normal organism biology beyond the regulation of neurotransmitter release. In this context, the increase, rather than decrease, of the paralysis recovery time of the double-mutant flies may result from the reduced ARI ligase activity, due to *ari*^{2} heterozygosity, upon other synaptic target proteins (*e.g.*, Vamp-7, among others, Fig. 3). Alternatively, the disequilibrium between the *ari*^{2} effects upon spontaneous *versus* evoked release (Figs. 5 and 6) and/or a

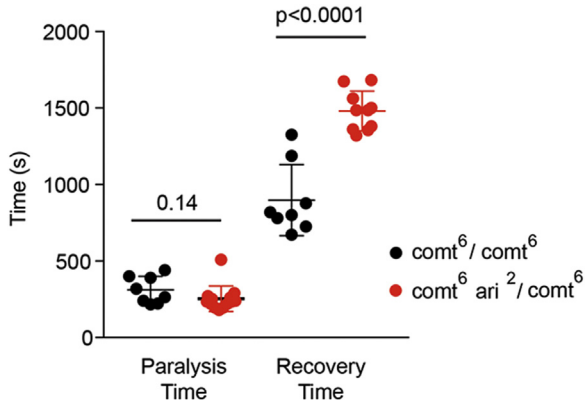

Figure 8. Genetic interaction between *ari²* and *comt⁶* mutants. Time to reach full paralysis in a 37 °C water bath of *comt⁶/comt⁶* females is not statically significant with respect to *comt⁶ ari²/comt⁶* (mean 311 ± 31 *versus* 253 ± 22; $p = 0.14$). The recovery time shows a strong increase in the later genotype, where three out of 13 individuals required more than 1 h to reach the recovery criterion (not included). Eventually, all flies fully recovered from temperature paralysis. On average, the mean recovery time was of 893 ± 82 and 1693 ± 116, *comt⁶/comt⁶ versus comt⁶ ari²/comt⁶*, respectively. These values are statistically different under the unpaired Student's *t* test; $p < 0.0001$. As control, *comt⁶ ari²/FM7* females were tested in parallel showing no paralysis during the whole time of the test.

putative differential effect upon excitatory *versus* inhibitory synapses could contribute to the phenotype change. These speculations, however, will require focused studies in the future.

Discussion

We identified 16 novel putative substrates of Ari-1 in *Drosophila* photoreceptor neurons *in vivo* by means of an unbiased proteomic approach. Remarkably, despite Ari-1 being recently shown to regulate the positioning of the cell nucleus in muscles *via* a direct interaction with Parkin (21), as well as to interact with some Parkin substrates (21, 23), there is no overlap between the substrates identified for Ari-1 and those previously identified for Parkin in flies (28). Taken together, the available data suggest that the 16 targets identified here are specifically regulated by Ari-1 in *Drosophila* photoreceptor neurons and that this E3 ligase has a wide functional repertoire.

We focused this study on Comt, an ATPase required for the maintenance of the neurotransmitter release (32). Ubiquitination of proteins involved in vesicle trafficking and neurotransmitter release had been previously reported (17, 25, 26, 43). Similarly, the importance of the ubiquitination machinery for the proper neuronal function has also been demonstrated (14, 16, 44, 45). The alterations produced on synaptic transmission by ubiquitination are typically attributed to an acute control of synaptic protein turnover (17, 46). However, many of these presynaptic proteins have been reported to be mainly mono- or di-ubiquitinated (25, 26), a type of ubiquitin modification that is not usually associated with protein degradation. In line with this, our results showed that Comt/NSF is preferentially mono-ubiquitinated by Ari-1/ARIH1, suggesting that Ari-1/ARIH1 could be regulating Comt/NSF activity, rather than its life span or expression levels.

Ari-1 mutations result in abnormal synaptic function at the larval stage, a result consistent with a regulatory function of NSF. All mutant alleles examined exhibit a reduced frequency of spontaneous synaptic release. In addition, *ari-1²* mutants exhibit a large calcium-dependent evoked release. Analysis of the mechanism for enhanced evoked release in *ari-1²* suggests that the primary defect consists in an increased probability of vesicle fusion in response to calcium entry in the presynaptic side. First, by comparing the amplitude and time course of spontaneously occurring postsynaptic events in mutant and control animals, we ruled out the possibility of a postsynaptic modification. Since no significant differences were found, we concluded that the receptor field size and kinetic properties of postsynaptic receptors are normal in the mutant.

The *ari-1* functional defects could result from alterations of synaptic transmission during development (47); therefore, we quantified the number of synaptic contacts, assuming that most release sites occur within varicosities (48). We did not observe any significant difference between mutant and control. Although this study does not include electron microscopy quantification of synaptic vesicles, our confocal microscopy and electrophysiology data point toward an upregulation of release from single synapses.

The failure analysis from single varicosities represents direct evidence that, at relatively low calcium concentrations, mutant terminals release more quanta than controls in response to an action potential. We further examined whether increased quantal release could be explained on the basis of more release sites being concentrated on mutant terminals. The focal recordings using saturating calcium concentrations argue against this possibility. When mutant terminals are exposed to high calcium, in order to increase the likelihood that all active zones within the bouton will release a quantum, EJP amplitudes in the mutant are indistinguishable from that of controls. These data suggest that the number of release sites in mutant and control terminals is similar and favor the hypothesis that, at physiological calcium concentrations, the probability of vesicle fusion upon calcium entry is increased in the mutant.

We found that *ari-1* mutants have opposite effects on spontaneous and evoked release. Classically, the two modes of vesicular release have been considered to represent a single exocytotic process that functions at different rates depending on the Ca^{2+} concentration. However, recent work challenges this idea and supports the alternative model where spontaneous and evoked response might come from different vesicles pools (49). Several experimental evidences indicate that both forms of release may represent separate fusion pathways (50–53). Employing a state-of-the-art optical imaging in larval NMJ, it has been shown that evoked and spontaneous release can be segregated across active zones. Thus, three types of active zones could be defined: those that only release vesicles in response to a rise of intracellular calcium (evoked release), a second population that only participates in spontaneous release, and a third small proportion (around 4%) that participates in both evoked and spontaneous release. This result advocates for a different molecular and spatial segregation of both modes of release (52).

Differential content or activity of regulatory SNARE binding proteins could discriminate between spontaneous and evoked release. It has been shown that the presence of the Vamp-7 isoform could participate in this differential release. Vamp-7 preferentially labels vesicles unresponsive to stimulation, and it colocalizes only partially with the endogenous synaptic vesicle glycoprotein Sv2 and the vesicular glutamate transporter Vglut1, suggesting that this vesicle pool does not support evoked transmitter release (51). Recently, it was shown that the double knockout mouse for Synaptobrevin genes, *syb1* and *syb2*, results in a total block of evoked release, while spontaneous release was increased in both frequency and quantal size without changes in the number of docked vesicles at the active zone (53), confirming the idea that evoked and spontaneous releases are differentially regulated. Interestingly, Vamp-7 was found by MS to be less ubiquitinated when Ari-1 is overexpressed (Fig. 3), suggesting that Ari-1 mutants could be favoring evoked release through NSF and reducing spontaneous release through Vamp7. Thus, Ari-1 could be acting as a repressor and activator of evoked and spontaneous release, respectively. All together, these results evidence a new layer of complexity over the actual fine-tuning of synaptic transmission. A physiological regulatory mechanism for both types of release has been recently demonstrated for inhibitory synapses at the trapezoid body, an important brain area in auditory integration. In this nucleus, activation of metabotropic glutamate receptor mGluR1 differentially modulates both spontaneous and evoked release in both GABAergic and Glycynergic synapses (54).

Early functional studies of NSF employing the fly thermosensitive mutant allele $comt^{ts17}$, have reported a reversible reduction of synaptic transmission. Consistent with a role of NSF on SNARE dissociation, this inhibition parallels an increase in the number of synaptic vesicles at the presynaptic terminal (55–57). At this point, we can only speculate how specifically Ari-1/ARIH1 regulates Comt/NSF activity within the presynaptic terminal. Opposite to the role of NSF mutant com^{st17}, which impairs SNARE complex disassembly (55), a change that enhances NSF functionality due to the lack of its ubiquitination would favor the dissociation of the so-called *trans*-SNARE complex. Further, this would build up the number of SNARE complexes assembled per vesicle, thus increasing the efficiency of fusion machinery in a Ca^{2+}-dependent manner. Consistent with this interpretation, it has been shown that fast release of a synaptic vesicle requires at least three SNARE complexes, whereas slower release may occur with fewer complexes (58).

Interestingly, some of the additional putative substrates identified are also related to synapse physiology and neurotransmitter release. PPO1 is an enzyme with L-DOPA monooxygenase activity, hence, may be involved in the metabolism of dopamine neurotransmitter (59). Similarly, GstO3 is involved in glutathione metabolism (60), another type of neurotransmitter (61). Vha44 and Vha68-1 are components of the vacuolar proton-pump ATPase (62), whose mutations have been reported to impair neurotransmitter release (63). Vha44 has also been described as an enhancer of Tau-induced neurotoxicity (64), and CG15117, orthologue of human GUSB, has been associated with neuropathological abnormalities (65). The long recovery time from paralysis observed in $comt^{6}$ $ari^{2}/comt^{6}$ females could result from the role of Ari-1 in the ubiquitination of these additional substrates, in addition to the role of Comt in tissues other than the nervous system.

The data reported here may be relevant in the context of Parkinson's disease. It should be noted that most Parkinson's-related genes encode proteins involved in vesicle recycling and neurotransmitter release at the synapse (66). Thus, the kinase LRRK2 phosphorylates NSF to enhance its ATPase activity upon the SNARE complex and facilitate its disassembly (7–9). Pathological mutations in this protein, such as G2019S, cause an excess of kinase activity (10) that interferes with vesicle recycling (11). Deregulated synaptic aggregates of α-Synuclein may target VAMP-2 hampering the formation of the SNARE complex (13, 67). Parkin is a structural relative of Ari-1, based on their common Cysteine rich C_3HC_4 motif (19), which is also at the origin of some forms of Parkinson's disease (68). All these genes and their corresponding mechanisms of activity sustain the scenario in which several types of Parkinson's disease seem to result from a defective activity of the synapse. In this context, the role of Ari-1/ARIH1 emerges as a mechanism to regulate a key component of the SNARE complex, Comt/NSF. Conceivably, Ari-1/ARIH1 may become a suitable target for either diagnosis or pharmacological treatment of Parkinson's and related diseases.

Experimental procedures

Fly strains and genetic procedures

The four $ari\text{-}1^{1-4}$ alleles have been previously described and sequenced (18), and the protein sequence can be found in the EMBL data bank under accession number #Q94981. The insertional duplication *Dp(1;3)JC153* (*Dp* for brevity) is routinely used to cover the lethality of *ari-1* and to demonstrate that the mutant phenotype is due to the gene *ari-1*, rather than to a putative second site mutation along the chromosome. *UAS-ari-1* flies, as well as flies overexpressing the $(^{bio}Ub)_6$-BirA construct in the *Drosophila* photoreceptor neurons under the control of the GMR-GAL4 driver (*GMR-Gal4, UAS-*$(^{bio}Ub)_6$*-BirA/CyO; TM2/TM6*), had been previously described (22, 26). *UAS-comt-GFP* flies, used for the overexpression of the *Drosophila* NSF1 protein, were obtained from Dr R. Ordway (Penn State University).

UAS-ari-1 flies were mated to *GMR-Gal4, UAS-*$(^{bio}Ub)_6$*-BirA/CyO; TM2/TM6* control flies to generate *GMR-Gal4, UAS-*$(^{bio}Ub)_6$*-BirA/CyO; UAS-ari-1/TM6* flies (abbreviated throughout the text as $ari\text{-}1^{OE}$). Control and $ari\text{-}1^{OE}$ flies were then mated to *UAS-comt-GFP* flies in order to generate *GMR-Gal4, UAS-*$(^{bio}Ub)_6$*-BirA/CyO; UAS-comt-GFP/TM6* (abbreviated throughout the text as *comt*), and *GMR-Gal4, UAS-*$(^{bio}Ub)_6$*-BirA/CyO; UAS-ari-1/UAS-comt-GFP* flies (abbreviated throughout the text as $ari\text{-}1^{OE}/comt$), respectively. Mixed-sex flies of 2–5 days old of each genotype (^{bio}Ub, ^{bio}ari, $^{bio}comt$ and $^{bio}ari/comt$) were frozen in liquid nitrogen and their heads were collected using a pair of sieves with a

nominal cutoff of 710 and 425 μm as previously described (26, 29). Fly heads were then stored at −80 °C until required. All fly lines were grown at 25 °C in 12 h light–dark cycles in standard *Drosophila* medium.

Plasmids and cloning procedures

FLAG-tagged ubiquitin (30) in pcDNA3.1 vector was generously provided by Dr Jose Antonio Rodríguez Pérez (University of the Basque Country-UPV/EHU, Spain). pFLAG-ARIH1^{WT} plasmid, overexpressing an N-terminally FLAG-tagged version of the wild-type human ARIH1 protein, was a gift from Dong-Er Zhang (Addgene plasmid # 17450; http://n2t.net/addgene:17450; RRID: Addgene_17450). A catalytically inactive version of ARIH1 was generated by site-directed mutagenesis of the active-site Cysteine (C357) to a Serine (pFLAG-ARIH1^{C357S}). The procedure was carried out with the QuickChange Site-Directed mutagenesis kit (Agilent Technologies), according to the manufacturer's instructions. The primers used for the mutagenesis were the following: 5′-GACAGACCATGTGATTAGAACCACCATCCT TCTCA-3′ and 5′-TGAGAAGGATGGTGGTTCTAATCA-CATGGTCTGTC-3′. Plasmid correct sequence was confirmed by sequencing at NZYtech (Portugal).

N-terminally GFP-tagged NSF plasmid (pEGFP-NSF) was generated by cloning NSF gene between KpnI and SmaI sites of the pEGFP-C1 vector (Clontech). For that, human NSF was amplified from pcDNA3-FLAG-NSF plasmid, a gift from Elisa Greggio (Addgene plasmid # 74924; http://n2t.net/addgene:74924; RRID: Addgene_74924), using the *NSF-forward* (5′-ACCGGTACCGCGGGCCGGAGCATGC-3′) and the *NSF-reverse* (5′-ACCCCCGGGTCAATCAAAATCAAGGGGGC-TAGC-3′) primers. In-frame position of NSF relative to GFP was confirmed by sequencing at NZYtech.

Cell culture and transfection

Human Embryonic Kidney cells (HEK293T) were cultured under standard conditions (37 °C, 5% CO_2) in Dulbecco's modified Eagle medium/nutrient mixture F-12 (DMEM/F-12) with GlutaMAX (Gibco), supplemented with 10% fetal bovine serum (Gibco), 100 U/ml of penicillin (Gibco) and 100 μg/ml of streptomycin (Gibco). About 6×10^5 cells were seeded in six-well plates for GFP pull-down assays. Next day, cells were cotransfected with 1 μg of pcDNA3.1-FLAG-ubiquitin, 1 μg of pEGFP-NSF, and either 1 μg of pFLAG-ARIH1^{WT} or pFLAG-ARIH1^{C357S} plasmids, using Lipofectamine 3000 reagent (Invitrogen) according to manufacturer's instructions. Cells were then harvested 24 h later and pellets frozen until at −80 °C until required.

Biotin pull-down assay

Biotin pull-downs (25) from *Drosophila* heads were performed as previously described (26). In brief, about 500 mg of heads of control and *ari-1*^{OE} flies was homogenized in 2.9 ml of *lysis buffer*. Lysates were centrifuged at 16,000*g* at 4 °C for 5 min and the supernatant applied to a *binding buffer*-equilibrated PD10 desalting column (GE Healthcare). Eluates, except 50 μl kept as input fraction, were incubated with 250 μl of NeutrAvidin agarose resin (Thermo Scientific) for 40 min at room temperature and further 2 h and 20 min at 4 °C with gentle rolling. The material bound to the resin was washed twice with *washing buffer* (*WB*) 1, thrice with *WB*2, once with *WB*3, thrice with *WB*4, once again with *WB*1, once with *WB*5, and thrice with *WB*6. The material that was still bound to the resin (*i.e.*, the ubiquitinated material) was eluted by heating the resin at 95 °C for 5 min in 125 μl of *elution buffer*. Finally, samples were centrifuged at 16,000*g* at room temperature for 2 min in a Vivaclear Mini 0.8 μm PES-micro-centrifuge filter unit (Sartorious) to discard the NeutrAvidin resin.

Buffer compositions for the biotin pulldown assays were as follows: *lysis buffer*, 8 M urea, 1% SDS, 1× PBS, 50 mM N-ethylmaleimide (Sigma), and a protease inhibitor cocktail (Roche); *biding buffer*, 3 M urea, 1 M NaCl, 0.25% SDS, 1× PBS and 50 mM N-ethylmaleimide; *WB1*, 8 M urea, 0.25 SDS, 1× PBS; *WB*2, 6 M guanidine-HCl, 1× PBS; *WB*3, 6.4 M urea, 1 M NaCl, 0.2% SDS, 1× PBS; *WB*4, 4 M urea, 1 M NaCl, 10% isopropanol, 10% ethanol, 0.2% SDS, 1× PBS; *WB*5, 8 M urea, 1% SDS, 1× PBS; *WB*6, 2% SDS, 1× PBS; *elution buffer*, 250 mM Tris-HCl, pH 7.5, 40% glycerol, 4% SDS, 0.2% bromophenol blue, and 100 mM dithiothreitol (DTT).

GFP pull-down assay

GFP pull-downs from HEK293T cells were performed as previously described (30, 31). In the case of fly samples, slight modifications were added to adapt the protocol to *Drosophila* heads. Briefly, about 100 mg of mixed-sex fly heads of *comt* and *ari-1*^{OE}*/comt* flies was homogenized in 400 μl of *lysis buffer*. Lysates were centrifuged once at 16,000*g* at room temperature for 1 min, in order to get rid of most of the *Drosophila* head fragments, and then centrifuged once again at 16,000*g* at 4 °C for 10 min. In total, 40 μl of the supernatants was kept as input, while 300 μl was diluted with 450 μl of *dilution buffer* to reduce their Triton concentration to 0.2% for a better binding. Diluted samples (750 μl) were then incubated with 40 μl of *dilution buffer*-washed GFP-Trap-A agarose beads suspension (Chromotek GmbH) for 2 h and 30 min at room temperature with gentle rolling. GFP beads were subsequently washed once with *dilution buffer*, thrice with *washing buffer*, and once with *SDS buffer*. Bound GFP-tagged Comt was eluted in 50 μl of *elution buffer* by heating at 95 °C for 10 min. Samples were centrifuged at 16,000*g* for 2 min and supernatant recovered, in order to get rid of the GFP-Trap-A agarose beads.

Buffer compositions for the GFP pull-down assays were as follows: *lysis buffer*, 50 mM Tris-HCl, pH 7.5, 150 mM NaCl, 1 mM EDTA, 0.5% Triton, 50 mM N-ethylmaleimide (Sigma), and 1× protease inhibitor cocktail (Roche); *dilution buffer*, 10 mM Tris-HCl, pH 7.5, 150 mM NaCl, 1 mM EDTA, 50 mM N-ethylmaleimide, and 1× protease inhibitor cocktail; *washing buffer*, 8 M urea, 1% SDS, 1× PBS; *elution buffer*, 250 mM Tris-HCl, pH 7.5, 40% glycerol, 4% SDS, 0.2% bromophenol blue, and 100 mM DTT.

In-gel trypsin digestion and peptide extraction

Eluates from biotin pull-down assays were concentrated in Vivaspin 500 centrifugal filter units (Sartorius) and resolved by

SDS-PAGE in 4–12% Bolt Bis-Tris precast gels (Invitrogen). Proteins were visualized with GelCode blue stain reagent (Invitrogen) and avidin monomers (∼15 kDa) and dimers (∼30 kDa), still present in the samples, as well as an endogenously biotinylated protein found at ∼130 kDa were excluded. For that, the gels were cut into the following slices: slice *A1* from ∼15 kDa to ∼25 kDa; slice *A2* from ∼30 kDa to 50 kDa; slice *B* from 50 kDa to ∼130 kDa, and slice *C* from ∼140 kDa to up to the gel. These four slices were then subjected to in-gel trypsin digestion as described previously (69). In brief, proteins were first reduced with DTT and then alkylated with chloroacetamide. Afterward, gel pieces were saturated with trypsin and incubated overnight at 37 °C. The resulting peptides were extracted from the gel, dried down in a vacuum centrifuge, and stored at −20 °C. Peptide mixtures were resuspended in 0.1% formic acid for LC-MS/MS analysis.

LC-MS/MS analysis

An EASY-nLC 1000 liquid chromatography system interfaced with a Q Exactive mass spectrometer (Thermo Scientific) *via* a nanospray flex ion source was employed for the mass spectrometric analyses. Peptides were loaded onto an Acclaim PepMap100 pre-column (75 μm × 2 cm, Thermo Scientific) connected to an Acclaim PepMap RSLC (50 μm × 15 cm, Thermo Scientific) analytical column. A 2 to 40% acetonitrile in 0.1% formic acid linear gradient, at a flow rate of 300 nl min^{-1} over 45 min, was used to elute peptides from the columns. The mass spectrometer was operated in positive ion mode. Full MS scans were acquired from *m/z* 300 to 1850 with a resolution of 70,000 at *m/z* 200. The ten most intense ions were fragmented by higher energy C-trap dissociation with normalized collision energy of 28. MS/MS spectra were recorded with a resolution of 17,500 at *m/z* 200. The maximum ion injection time was 120 ms for both survey and MS/MS scans, whereas automatic gain control target values of 3×10^6 and 5×10^5 were used for survey and MS/MS scans, respectively. Dynamic exclusion was applied for 45 s to avoid repeated sequencing of peptides. Singly charged ions or ions with unassigned charge state were also excluded from MS/MS. Data were acquired using Xcalibur software (Thermo Scientific).

Data processing and bioinformatics analysis

Acquired raw data files were processed with the MaxQuant (70) software (version 1.5.3.17) using the internal search engine Andromeda (71) and tested against the UniProt database filtered for *Drosophila melanogaster* entries (release 2015_11; 43,712 entries). Spectra originated from the different slices corresponding to the same biological sample were combined. Carbamidomethylation (C) was set as a fixed modification, whereas methionine oxidation, protein N-terminal acetylation, and lysine GlyGly (not C-term) were defined as variable modifications. Mass tolerance was set to 8 and 20 ppm at the MS and MS/MS level, respectively. Enzyme specificity was set to trypsin, allowing for a maximum of three missed cleavages. Match between runs option was enabled with 1.5 min match time window and 20 min alignment window to match identification across samples. The minimum peptide length was set to seven amino acids. The false discovery rate for peptides and proteins was set to 1%. Normalized spectral protein LFQ intensities were calculated using the MaxLFQ algorithm (33).

Western blot analysis

In total, 4–12% gradient Bolt Bis-Tris Plus precast gels (Invitrogen) were used for SDS-PAGE. Proteins were transferred to PVDF membranes using the iBlot system (Invitrogen). Following blocking, primary and secondary antibody incubation, membranes were developed either by chemiluminescence, using the Clarity Western ECL Substrate kit (Bio-Rad), or by near-infrared fluorescence. In both cases membranes were developed using the ChemiDoc MP Imaging system (Bio-Rad). Biotinylated proteins and, thus, ubiquitinated proteins were detected with goat anti-biotin horseradish peroxidase (HRP)-conjugated antibody (Cell Signaling Technology, Cat# 7075) at 1:1000. A mouse monoclonal anti-BirA antibody (Novus Biologicals, Cat# NBP2-59939) at 1:500 was used to detect BirA protein. A mouse monoclonal anti-GFP antibody (Roche, Cat# 11814460001) at 1:1000, as well as a rabbit polyclonal anti-GFP antibody (Santa Cruz Biotechnology, Cat# sc-8334) at 1:1000, was used to detect fly Comt-GFP and human GFP-NSF proteins. A mouse monoclonal anti-FLAG M2 HRP-conjugated antibody (Sigma; Cat# A8592) at 1:1000 was used to detect FLAG-tagged ubiquitin, as well as wild-type and catalytically inactive FLAG-tagged ARIH1. A mouse monoclonal anti-β-Tubulin (Developmental Studies Hybridoma Bank, Cat# E7-c) at 1:1000 was used for loading control. Goat anti-rabbit HRP-labeled antibody (Cell Signalling, Cat# 7074) at 1:4000 and goat anti-mouse IRDye-800CW (LI-COR Biosciences, Cat# 926-32210) at 1:8000 were used as secondary antibodies.

Larval neuromuscular preparation

Mature third instar larvae at the wandering stage were selected for electrophysiological recordings. As previously described (72), they were pinned down onto a Sylgard-coated experimental chamber and cut open along the dorsal midline in an extracellular solution containing 100 mM NaCl, 5 mM KCl, 20 mM $MgCl_2$, 5 mM HEPES, and 115 mM Sucrose (pH 7.3). After pinning the cuticle flat, all internal organs were removed to expose the body-wall muscle layer, leaving only the central nervous system connected to the muscles through the segmental nerves. These were severed near the CNS and their cut-open ends sucked into a fired-polished glass suction pipette filled with extracellular saline solution. The preparations were then transferred to the microscope for electrophysiological recordings and viewed with a 40× water immersion objective under Nomarski optics. All experiments were performed at room temperature (21–23 °C) on ventrolateral muscle fibers from segments A2–A5.

Electrophysiology

Spontaneous (mEJCs) and nerve-evoked (EJCs) junctional currents were recorded from muscle fibers 6 and 12, using an

Axoclamp-2A amplifier in two-electrode voltage-clamp (TEVC) mode. Short-shank pipettes (8–10 MΩ resistance when filled with 1 M KCl solution) were pulled on a Flaming-Brown puller (Sutter Instruments) from thin-wall borosilicate glass (World Precision Instruments). Upon establishing TEVC, the feedback gain control of the amplifier was adjusted, while monitoring the current response to repetitive hyperpolarizing voltage commands, as to obtain a minimal clamp settling time (∼2 ms) without introducing oscillations or excess noise in the current trace. The holding current, always less than −5 nA for a holding potential of −80 mV, was continuously monitored throughout the experiment. Current signals were low-pass filtered at 500–1000 Hz, digitized, and stored in a computer for further off-line analysis using a computer program (SNAP) written in our lab. Current signals were recorded in extracellular solution to which calcium had been added as a chloride salt to attain the desired final concentration (0–1.2 mM) as indicated in the text. The number of mEJCs acquired in free-run mode over 3-min periods was counted in order to determine the average frequency of spontaneous release. To compare the mEJCs amplitude distribution between genotypes, data recorded from different animals (200 consecutive events from each animal) of the same genotype were pooled into single data sets.

Evoked EJCs were elicited in voltage-clamped muscle fibers by delivering single pulses (100–200 μs) from a stimulator (Cibertec Stimulator CS 20). The stimulus intensity was adjusted slightly over the level required to recruit both motor axons innervating ventrolateral muscle fibers to produce a compound EJC. A mean EJC response for each muscle fiber sampled was obtained by averaging 25 to 50 consecutive responses elicited at 0.2 Hz. Extracellular focal synaptic signals from single boutons were recorded by placing extracellular pipettes (fired polished, 2–5 μm inner diameter) over type Is boutons, easily identified under Nomarski optics, and applying very gentle suction, which was released prior to the beginning of the experiment. Only those boutons showing no visible signs of damage after the experiment were considered in the analysis. In those experiments designed to assess single-terminal failure rates, whole-muscle EJPs were simultaneously recorded with intracellular electrodes in current-clamp mode, as to detect any possible stimulation failure susceptible of being wrongly classed as a release failure. Pooled data in the text are presented as mean ± SEM. The Student's *t* test with a level of significance $p < 0.05$ was routinely used to compare mean values between different genotypes, except when comparing mEJC amplitude distributions, where a Kolmogorov–Smirnov test was used.

Immunohistochemical procedures

Third instar larvae were dissected open as described and then fixed for 30 min in freshly made 4% paraformaldehyde in Ca^{2+}-free PBS containing 5 mM EGTA. After a series of washes with PBS, the larvae were incubated in PBT (0.1% Triton in PBS) with 2% BSA and 5% goat serum, added for 2 h at room temperature. Specimens were next incubated in mouse monoclonal anti-CSP antibody (mAb49) at 1:100 (73, 74), overnight at 4 °C in PBT, thoroughly washed in PBT, and then incubated in secondary anti-mouse antibody (1:1000) conjugated to Cy2 (Jackson Immuno Research, cat# 115-225-146), for 1 h at room temperature. Preparations were mounted on PBS:glycerol (1:1) and viewed under confocal microscopy.

Temperature-sensitive paralysis and recovery

Adult females aged 3–7 days were tested individually in vials on a 37 °C water bath. The criterion for paralysis was the fly's cessation of movement in all appendages and loss of standing position. The criterion for recovery was the ability to stand up on the six legs. Flies were anesthetized under CO_2, allowed to recover for 1 h, and monitored visually while the vial was in the bath. Once paralyzed, the vial was kept in the 37 °C bath for 1 min before being taken out to room temperature to measure fly's recovery time. Cultures and crosses were raised at room temperature.

Experimental design and statistical analyses

Biotin pull-downs

Experiments were performed in triplicate, where 500 mg of mixed-sex fly heads of each genotype (control and *ari-1*^{OE}) for each replica was used. The amount of heads was set to 500 mg to maximize the amount of ubiquitinated material that is purified and to minimize the amount of reagents that are used. This amount of heads ensures the isolation of enough ubiquitinated material for MS analyses, but does not saturate the PD10 columns, so only one per sample is used. Additionally, the amount of NeutrAvidin beads used can be reduced significantly. After MS analysis, MaxQuant output data from control and *ari-1*^{OE} samples were analyzed with the Perseus module (version 1.5.6.0) (75) in order to determine the proteins and GlyGly peptides significantly enriched in each of the genotypes. First, contaminants, reverse hits, as well as proteins and GlyGly peptides with no intensity were removed. Later, during the analysis of proteins, those only identified by site and/or with no unique peptides were also removed. LFQ intensities were used to determine the abundance of proteins, while raw intensities, normalized by median subtraction, were used for GlyGly peptides. Missing intensity values were replaced with values from a normal distribution (width 0.3 and down shift 1.8), meant to simulate expression below the detection limit (75). Statistically significant changes in protein and GlyGly peptide abundance were assessed by two-tailed Student's *t* test. Proteins and GlyGly peptides displaying a fold change above 2 with a *p*-value below 0.05 were selected for further analysis. The selected proteins and peptides were further filtered based on the number of unique peptides and/or on the number of imputed values. For further analyses, we only considered the statistical significance of those proteins that (i) had no imputed values in any of the three replicas of at least one of the conditions or (ii) had a maximum of one imputed value in each of the conditions.

GFP pull-downs

Experiments were performed in triplicate, where 100 mg of mixed-sex fly heads of each genotype (*comt* and *ari-1*^{OE}*/comt*)

for each replica was used. The amount of heads was determined as the minimum amount needed to saturate 40 µl of GFP-Trap_A beads. Experiments were also performed in triplicate from cell samples, for which 25 µl of GFP-Trap_A beads were used per replica as previously described (31). Semiquantification of dual-color western blots was performed with Image Lab software (Bio-Rad). Ubiquitination levels of GFP-tagged Comt and GFP-NSF were normalized to the nonmodified fractions. Statistical significance of the ubiquitination levels was then determined by two-tailed Student's *t* test using GraphPad software.

Electrophysiology statistical analysis

All statistical analyses were done by the GraphPad Prism version 7.0 (GraphPad Software). Data are presented as mean ± SEM unless otherwise noted. Two-tailed Student's *t* test was used to assess differences between control and other groups. One-way ANOVA was used for analysis of data from three or more groups followed by two-tailed Student's *t* test, coefficients of significance are included in the figures.

Data availability

Original mass spectrophotometry data are deposited in the PRIDE repository under accession number PXD022701. All other original data are available in the main text and figures.

Supporting information—This article contains supporting information.

Acknowledgments—We thank the Bloomington *Drosophila* Stock Center (NIH P40OD018537), the Vienna *Drosophila* Resource Center, and Prof. Richard Ordway for fly strains. The technical help of Ms Esther Seco is most appreciated. The authors are also grateful of the technical support provided by Kerman Aloria from the UPV/EHU SGIker, which is supported with European funding (ERDF and ESF).

Author contributions—J. R. design, execution, analysis of ubiquitination experiments, and text writing; N. O. design and execution of bioinformatics analysis; M. M. analysis of electrophysiology experiments and text writing; I. M.-P. design and execution of electrophysiology experiments; U. M. design and analysis of ubiquitination experiments and text writing; A. F. design and execution of genetic experiments and text writing.

Funding and additional information—This research was funded by grants BFU2015-65685 and PGC2018-094630-B-100 from the Spanish Ministry of Economy to A. F. and grant SAF2016-76898-P from the Spanish Ministry of Economy cofinanced with FEDER funds to U. M. J. R. was supported with a postdoctoral research fellowship from the University of the Basque Country (UPV/EHU).

Conflict of interest—The authors declare that they have no conflicts of interest with the contents of this article.

Abbreviations—The abbreviations used are: Ari-1, *Drosophila* Ariadne-1; ARIH1, human Ariadne-1; Comt, Comatose; DTT, dithiothreitol; EJP, excitatory junctional potential; LC-MS/MS, liquid chromatography with tandem mass spectrometry; LFQ, label-free quantification; LRRK2, Leucine-rich repeat Serine/Threonine-protein kinase 2; mEJC, mini excitatory junctional current; NMJ, neuromuscular junctions; NSF, N-ethylmaleimide sensitive factor; RRP, readily releasable pool; SNAP, Soluble NSF attachment proteins; SNARE, SNAP receptor; v-SNARE, vesicle membrane SNARE protein; t-SNARE, plasma membrane SNARE protein; TEVC, two-electrode voltage clamp conditions; VAMP, vesicle-associated membrane protein.

References

1. Söllner, T., Whiteheart, S. W., Brunner, M., Erdjument-Bromage, H., Geromanos, S., Tempst, P., and Rothman, J. E. (1993) SNAP receptors implicated in vesicle targeting and fusion. *Nature* **362**, 318–324
2. Jahn, R., and Scheller, R. H. (2006) SNAREs–engines for membrane fusion. *Nat. Rev. Mol. Cell Biol.* **7**, 631–643
3. Littleton, J. T. (2000) A genomic analysis of membrane trafficking and neurotransmitter release in Drosophila. *J. Cell Biol.* **150**, F77–F82
4. Südhof, T. C. (2013) Neurotransmitter release: The last millisecond in the life of a synaptic vesicle. *Neuron* **80**, 675–690
5. Yu, W., Kawasaki, F., and Ordway, R. W. (2011) Activity-dependent interactions of NSF and SNAP at living synapses. *Mol. Cell. Neurosci.* **47**, 19–27
6. Bridi, J. C., and Hirth, F. (2018) Mechanisms of α-synuclein induced synaptopathy in Parkinson's disease. *Front. Neurosci.* **12**, 80
7. Shin, N., Jeong, H., Kwon, J., Heo, H. Y., Kwon, J. J., Yun, H. J., Kim, C. H., Han, B. S., Tong, Y., Shen, J., Hatano, T., Hattori, N., Kim, K.-S., Chang, S., and Seol, W. (2008) LRRK2 regulates synaptic vesicle endocytosis. *Exp. Cell Res.* **314**, 2055–2065
8. Berger, Z., Smith, K. A., and Lavoie, M. J. (2010) Membrane localization of LRRK2 is associated with increased formation of the highly active LRRK2 dimer and changes in its phosphorylation. *Biochemistry* **49**, 5511–5523
9. Belluzzi, E., Gonnelli, A., Cirnaru, M. D., Marte, A., Plotegher, N., Russo, I., Civiero, L., Cogo, S., Carrion, M. P., Franchin, C., Arrigoni, G., Beltramini, M., Bubacco, L., Onofri, F., Piccoli, G., *et al.* (2016) LRRK2 phosphorylates pre-synaptic N-ethylmaleimide sensitive fusion (NSF) protein enhancing its ATPase activity and SNARE complex disassembling rate. *Mol. Neurodegener* **11**, 1
10. Rudenko, I. N., and Cookson, M. R. (2014) Heterogeneity of leucine-rich repeat kinase 2 mutations: Genetics, mechanisms and therapeutic implications. *Neurotherapeutics* **11**, 738–750
11. Piccoli, G., Condliffe, S. B., Bauer, M., Giesert, F., Boldt, K., De Astis, S., Meixner, A., Sarioglu, H., Vogt-Weisenhorn, D. M., Wurst, W., Gloeckner, C. J., Matteoli, M., Sala, C., and Ueffing, M. (2011) LRRK2 controls synaptic vesicle storage and mobilization within the recycling pool. *J. Neurosci.* **31**, 2225–2237
12. Burré, J., Sharma, M., and Südhof, T. C. (2018) Cell biology and pathophysiology of α-synuclein. *Cold Spring Harb. Perspect. Med.* **8**, a024091
13. Wang, C., Ma, Z., Yan, D. Y., Liu, C., Deng, Y., Liu, W., Xu, Z.-F., and Xu, B. (2018) Alpha-synuclein and calpains disrupt SNARE-mediated synaptic vesicle fusion during manganese exposure in SH-SY5Y cells. *Cells* **7**, 258
14. Hallengren, J., Chen, P.-C., and Wilson, S. M. (2013) Neuronal ubiquitin homeostasis. *Cell Biochem. Biophys.* **67**, 67–73
15. Swatek, K. N., and Komander, D. (2016) Ubiquitin modifications. *Cell Res* **26**, 399–422
16. Rinetti, G. V., and Schweizer, F. E. (2010) Ubiquitination acutely regulates presynaptic neurotransmitter release in mammalian neurons. *J. Neurosci.* **30**, 3157–3166
17. Speese, S. D., Trotta, N., Rodesch, C. K., Aravamudan, B., and Broadie, K. (2003) The ubiquitin proteasome system acutely regulates presynaptic protein turnover and synaptic efficacy. *Curr. Biol.* **13**, 899–910
18. Aguilera, M., Oliveros, M., Martínez-Padrón, M., Barbas, J. A., and Ferrús, A. (2000) Ariadne-1: A vital Drosophila gene is required in development and defines a new conserved family of ring-finger proteins. *Genetics* **155**, 1231–1244

19. Marín, I., and Ferrús, A. (2002) Comparative genomics of the RBR family, including the Parkinson's disease-related gene parkin and the genes of the ariadne subfamily. *Mol. Biol. Evol.* **19**, 2039–2050
20. Tan, N. G. S., Ardley, H. C., Scott, G. B., Rose, S. A., Markham, A. F., and Robinson, P. A. (2003) Human homologue of ariadne promotes the ubiquitylation of translation initiation factor 4E homologous protein, 4EHP. *FEBS Lett.* **554**, 501–504
21. Tan, K. L., Haelterman, N. A., Kwartler, C. S., Regalado, E. S., Lee, P. T., Nagarkar-Jaiswal, S., Guo, D. C., Duraine, L., Wangler, M. F., University of Washington Center for Mendelian Genomics, Bamshad, M. J., Nickerson, D. A., Lin, G., Milewicz, D. M., and Bellen, H. J. (2018) Ari-1 regulates myonuclear organization together with parkin and is associated with aortic aneurysms. *Dev. Cell.* **45**, 226–244.e8
22. Gradilla, A. C., Mansilla, A., and Ferrús, A. (2011) Isoform-specific regulation of a steroid hormone nuclear receptor by an E3 ubiquitin ligase in Drosophila melanogaster. *Genetics* **189**, 871–883
23. Parelkar, S. S., Cadena, J. G., Kim, C., Wang, Z., Sugal, R., Bentley, B., Moral, L., Ardley, H. C., and Schwartz, L. M. (2012) The parkin-like human homolog of Drosophila ariadne-1 (HHARI) can induce aggresome formation in mammalian cells and is immunologically detectable in Lewy bodies. *J. Mol. Neurosci.* **46**, 109–121
24. Ramirez, J., Elu, N., Martinez, A., Lectez, B., and Mayor, U. (2017) *In vivo* strategies to isolate and characterize the neuronal ubiquitinated proteome *Current Proteomic Approaches Applied to Brain Function*. Neuromethods, Humana Press, New York, NY: 179–189
25. Franco, M., Seyfried, N. T., Brand, A. H., Peng, J., and Mayor, U. (2011) A novel strategy to isolate ubiquitin conjugates reveals wide role for ubiquitination during neural development. *Mol. Cell Proteomics* **10**. M110.002188
26. Ramirez, J., Martinez, A., Lectez, B., Lee, S. Y., Franco, M., Barrio, R., Dittmar, G., and Mayor, U. (2015) Proteomic analysis of the ubiquitin landscape in the Drosophila embryonic nervous system and the adult photoreceptor cells. *PLoS One* **10**, e0139083
27. Beckett, D., Kovaleva, E., and Schatz, P. J. (1999) A minimal peptide substrate in biotin holoenzyme synthetase-catalyzed biotinylation. *Protein Sci.* **8**, 921–929
28. Martinez, A., Lectez, B., Ramirez, J., Popp, O., Sutherland, J. D., Urbé, S., Dittmar, G., Clague, M. J., and Mayor, U. (2017) Quantitative proteomic analysis of Parkin substrates in Drosophila neurons. *Mol. Neurodegener* **12**, 29
29. Ramirez, J., Lectez, B., Osinalde, N., Sivá, M., Elu, N., Aloria, K., Procházková, M., Perez, C., Martínez-Hernández, J., Barrio, R., Šašková, K. G., Arizmendi, J. M., and Mayor, U. (2018) Quantitative proteomics reveals neuronal ubiquitination of Rngo/Ddi1 and several proteasomal subunits by Ube3a, accounting for the complexity of Angelman syndrome. *Hum. Mol. Genet.* **27**, 1955–1971
30. Lee, S. Y., Ramirez, J., Franco, M., Lectez, B., Gonzalez, M., Barrio, R., and Mayor, U. (2014) Ube3a, the E3 ubiquitin ligase causing Angelman syndrome and linked to autism, regulates protein homeostasis through the proteasomal shuttle Rpn10. *Cell. Mol. Life Sci.* **71**, 2747–2758
31. Elu, N., Osinalde, N., Beaskoetxea, J., Ramirez, J., Lectez, B., Aloria, K., Rodriguez, J. A., Arizmendi, J. M., and Mayor, U. (2019) Detailed dissection of UBE3A-mediated DDI1 ubiquitination. *Front. Physiol.* **10**, 534
32. Ordway, R. W., Pallanck, L., and Ganetzky, B. (1994) Neurally expressed Drosophila genes encoding homologs of the NSF and SNAP secretory proteins. *Proc. Natl. Acad. Sci. U. S. A.* **91**, 5715–5719
33. Cox, J., Hein, M. Y., Luber, C. A., Paron, I., Nagaraj, N., and Mann, M. (2014) Accurate proteome-wide label-free quantification by delayed Normalization and maximal peptide ratio extraction, termed MaxLFQ. *Mol. Cell Proteomics* **13**, 2513–2526
34. Chandler, C. S., and Ballard, F. J. (1985) Distribution and degradation of biotin-containing carboxylases in human cell lines. *Biochem. J.* **232**, 385–393
35. Peng, J., Schwartz, D., Elias, J. E., Thoreen, C. C., Cheng, D., Marsischky, G., Roelofs, J., Finley, D., and Gygi, S. P. (2003) A proteomics approach to understanding protein ubiquitination. *Nat. Biotechnol.* **21**, 921–926
36. Haglund, K., Di Fiore, P. P., and Dikic, I. (2003) Distinct monoubiquitin signals in receptor endocytosis. *Trends Biochem. Sci.* **28**, 598–603
37. Husnjak, K., and Dikic, I. (2012) Ubiquitin-binding proteins: Decoders of ubiquitin-mediated cellular functions. *Annu. Rev. Biochem.* **81**, 291–322
38. Garcia-Barcena, C., Osinalde, N., Ramirez, J., and Mayor, U. (2020) How to inactivate human ubiquitin E3 ligases by mutation. *Front. Cell Dev. Biol* **8**, 39
39. Brunger, A. T., Choi, U. B., Lai, Y., Leitz, J., White, K. I., and Zhou, Q. (2019) The pre-synaptic fusion machinery. *Curr. Opin. Struct. Biol.* **54**, 179–188
40. Goda, Y., and Stevens, C. F. (1998) Readily releasable pool size changes associated with long term depression. *Proc. Natl. Acad. Sci. U. S. A.* **95**, 1283–1288
41. Schuster, C. M., Davis, G. W., Fetter, R. D., and Goodman, C. S. (1996) Genetic dissection of structural and functional components of synaptic plasticity. II. Fasciclin II controls presynaptic structural plasticity. *Neuron* **17**, 655–667
42. Mallart, A. (1993) Calcium-dependent modulation of the facilitation of transmitter release at neuromuscular junctions of Drosophila. *J. Physiol. Paris.* **87**, 83–88
43. Na, C. H., Jones, D. R., Yang, Y., Wang, X., Xu, Y., and Peng, J. (2012) Synaptic protein ubiquitination in rat brain revealed by antibody-based ubiquitome analysis. *J. Proteome Res.* **11**, 4722–4732
44. Yi, J. J., and Ehlers, M. D. (2007) Emerging roles for ubiquitin and protein degradation in neuronal function. *Pharmacol. Rev.* **59**, 14–39
45. Schwarz, L. A., and Patrick, G. N. (2012) Ubiquitin-dependent endocytosis, trafficking and turnover of neuronal membrane proteins. *Mol. Cell. Neurosci.* **49**, 387–393
46. Yao, I., Takagi, H., Ageta, H., Kahyo, T., Sato, S., Hatanaka, K., Fukuda, Y., Chiba, T., Morone, N., Yuasa, S., Inokuchi, K., Ohtsuka, T., Macgregor, G. R., Tanaka, K., and Setou, M. (2007) SCRAPPER-dependent ubiquitination of active zone protein RIM1 regulates synaptic vesicle release. *Cell* **130**, 943–957
47. Babcock, D. T., Shen, W., and Ganetzky, B. (2015) A neuroprotective function of NSF1 sustains autophagy and lysosomal trafficking in Drosophila. *Genetics* **199**, 511–522
48. Atwood, H. L., Govind, C. K., and Wu, C. F. (1993) Differential ultrastructure of synaptic terminals on ventral longitudinal abdominal muscles in Drosophila larvae. *J. Neurobiol.* **24**, 1008–1024
49. Kavalali, E. T. (2015) The mechanisms and functions of spontaneous neurotransmitter release. *Nat. Rev. Neurosci.* **16**, 5–16
50. Deitcher, D. L., Ueda, A., Stewart, B. A., Burgess, R. W., Kidokoro, Y., and Schwarz, T. L. (1998) Distinct requirements for evoked and spontaneous release of neurotransmitter are revealed by mutations in the Drosophila gene neuronal-synaptobrevin. *J. Neurosci.* **18**, 2028–2039
51. Hua, Z., Leal-Ortiz, S., Foss, S. M., Waites, C. L., Garner, C. C., Voglmaier, S. M., and Edwards, R. H. (2011) v-SNARE composition distinguishes synaptic vesicle pools. *Neuron* **71**, 474–487
52. Melom, J. E., Akbergenova, Y., Gavornik, J. P., and Littleton, J. T. (2013) Spontaneous and evoked release are independently regulated at individual active zones. *J. Neurosci.* **33**, 17253–17263
53. Liu, Y., Sugiura, Y., Südhof, T. C., and Lin, W. (2019) Ablation of all synaptobrevin vSNAREs blocks evoked but not spontaneous neurotransmitter release at neuromuscular synapses. *J. Neurosci.* **39**, 6049–6066
54. Curry, R. J., Peng, K., and Lu, Y. (2018) Neurotransmitter- and release-mode-specific modulation of inhibitory transmission by group I metabotropic glutamate receptors in central auditory neurons of the mouse. *J. Neurosci.* **38**, 8187–8199
55. Littleton, J. T., Barnard, R. J., Titus, S. A., Slind, J., Chapman, E. R., and Ganetzky, B. (2001) SNARE-complex disassembly by NSF follows synaptic-vesicle fusion. *Proc. Natl. Acad. Sci. U. S. A.* **98**, 12233–12238
56. Littleton, J. T., Chapman, E. R., Kreber, R., Garment, M. B., Carlson, S. D., and Ganetzky, B. (1998) Temperature-sensitive paralytic mutations demonstrate that synaptic exocytosis requires SNARE complex assembly and disassembly. *Neuron* **21**, 401–413
57. Kawasaki, F., Mattiuz, A. M., and Ordway, R. W. (1998) Synaptic physiology and ultrastructure in comatose mutants define an *in vivo* role for NSF in neurotransmitter release. *J. Neurosci.* **18**, 10241–10249
58. Mohrmann, R., de Wit, H., Verhage, M., Neher, E., and Sørensen, J. B. (2010) Fast vesicle fusion in living cells requires at least three SNARE complexes. *Science* **330**, 502–505

59. Li, X., Ma, M., Liu, F., Chen, Y., Lu, A., Ling, Q.-Z., Li, J., Beerntsen, B. T., Yu, X.-Q., Liu, C., and Ling, E. (2012) Properties of Drosophila melanogaster prophenoloxidases expressed in Escherichia coli. *Dev. Comp. Immunol.* **36**, 648–656
60. Saisawang, C., Wongsantichon, J., and Ketterman, A. J. (2012) A preliminary characterization of the cytosolic glutathione transferase proteome from Drosophila melanogaster. *Biochem. J.* **442**, 181–190
61. Oja, S. S., Janáky, R., Varga, V., and Saransaari, P. (2000) Modulation of glutamate receptor functions by glutathione. *Neurochem. Int.* **37**, 299–306
62. Allan, A. K., Du, J., Davies, S. A., and Dow, J. A. T. (2005) Genome-wide survey of V-ATPase genes in Drosophila reveals a conserved renal phenotype for lethal alleles. *Physiol. Genomics.* **22**, 128–138
63. Hiesinger, P. R., Fayyazuddin, A., Mehta, S. Q., Rosenmund, T., Schulze, K. L., Zhai, R. G., Verstreken, P., Cao, Y., Zhou, Y., Kunz, J., and Bellen, H. J. (2005) The v-ATPase V0 subunit a1 is required for a late step in synaptic vesicle exocytosis in Drosophila. *Cell* **121**, 607–620
64. Blard, O., Feuillette, S., Bou, J., Chaumette, B., Frébourg, T., Campion, D., and Lecourtois, M. (2007) Cytoskeleton proteins are modulators of mutant tau-induced neurodegeneration in Drosophila. *Hum. Mol. Genet.* **16**, 555–566
65. Bar, S., Prasad, M., and Datta, R. (2018) Neuromuscular degeneration and locomotor deficit in a Drosophila model of mucopolysaccharidosis VII is attenuated by treatment with resveratrol. *Dis. Model Mech.* **11**. dmm036954
66. Selvaraj, S., and Piramanayagam, S. (2019) Impact of gene mutation in the development of Parkinson's disease. *Genes Dis.* **6**, 120–128
67. Stefanis, L. (2012) α-Synuclein in Parkinson's disease. *Cold Spring Harb. Perspect. Med.* **2**, a009399
68. Shimura, H., Hattori, N., Kubo, S. i, Mizuno, Y., Asakawa, S., Minoshima, S., Shimizu, N., Iwai, K., Chiba, T., Tanaka, K., and Suzuki, T. (2000) Familial Parkinson disease gene product, parkin, is a ubiquitin-protein ligase. *Nat. Genet.* **25**, 302–305
69. Osinalde, N., Sánchez-Quiles, V., Akimov, V., Blagoev, B., and Kratchmarova, I. (2015) SILAC-based quantification of changes in protein tyrosine phosphorylation induced by Interleukin-2 (IL-2) and IL-15 in T-lymphocytes. *Data Brief* **5**, 53–58
70. Cox, J., and Mann, M. (2008) MaxQuant enables high peptide identification rates, individualized p.p.b.-range mass accuracies and proteome-wide protein quantification. *Nat. Biotech.* **26**, 1367–1372
71. Cox, J., Neuhauser, N., Michalski, A., Scheltema, R. A., Olsen, J. V., and Mann, M. (2011) Andromeda: A peptide search engine integrated into the MaxQuant environment. *J. Proteome Res.* **10**, 1794–1805
72. Martínez-Padrón, M., and Ferrús, A. (1997) Presynaptic recordings from Drosophila: Correlation of macroscopic and single-channel K+ currents. *J. Neurosci.* **17**, 3412–3424
73. Buchner, E., Bader, R., Buchner, S., Cox, J., Emson, P. C., Flory, E., Heizmann, C. W., Hemm, S., Hofbauer, A., and Oertel, W. H. (1988) Cell-specific immuno-probes for the brain of normal and mutant Drosophila melanogaster. I. Wildtype visual system. *Cell Tissue Res.* **253**, 357–370
74. Zinsmaier, K. E., Hofbauer, A., Heimbeck, G., Pflugfelder, G. O., Buchner, S., and Buchner, E. (1990) A cysteine-string protein is expressed in retina and brain of Drosophila. *J. Neurogenet.* **7**, 15–29
75. Tyanova, S., Temu, T., Sinitcyn, P., Carlson, A., Hein, M. Y., Geiger, T., Mann, M., and Cox, J. (2016) The Perseus computational platform for comprehensive analysis of (prote)omics data. *Nat. Methods* **13**, 731–740